Atmos. Chem. Phys. Discuss., 14, 21975–22043, 2014
www.atmos-chem-phys-discuss.net/14/21975/2014/
doi:10.5194/acpd-14-21975-2014

Atmospheric Chemistry and Physics Discussions

Aerosol–cloud interactions studied with the chemistry-climate model EMAC

D. Y. Chang[1], **H. Tost**[2], **B. Steil**[1], **and J. Lelieveld**[1,3]

[1]Max Planck Institute for Chemistry, Mainz, Germany
[2]Johannes Gutenberg University, Mainz, Germany
[3]The Cyprus Institute, Nicosia, Cyprus

Received: 31 July 2014 – Accepted: 12 August 2014 – Published: 27 August 2014

Correspondence to: D. Y. Chang (dongyeong.chang@mpic.de)

Published by Copernicus Publications on behalf of the European Geosciences Union.

Abstract

This study uses the EMAC atmospheric chemistry-climate model to simulate cloud properties and estimate cloud radiative effects induced by aerosols. We have tested two prognostic cloud droplet nucleation parameterizations, i.e., the standard STN (osmotic coefficient model) and hybrid (HYB, replacing the osmotic coefficient by the κ hygroscopicity parameter) schemes to calculate aerosol hygroscopicity and critical supersaturation, and consider aerosol–cloud feedbacks with a focus on warm clouds. Both prognostic schemes (STN and HYB) account for aerosol number, size and composition effects on droplet nucleation, and are tested in combination with two different cloud cover parameterizations, i.e., a relative humidity threshold and a statistical cloud cover scheme (RH-CLC and ST-CLC).

The use of either STN and HYB leads to very different cloud radiative effects, particularly over the continents. The STN scheme predicts highly effective CCN activation in warm clouds and hazes/fogs near the surface. The enhanced CCN activity increases the cloud albedo effect of aerosols and cools the Earth's surface. The cooler surface enhances the hydrostatic stability of the lower continental troposphere and thereby reduces convection and convective precipitation. In contrast, the HYB simulations calculate lower, more realistic CCN activation and consequent cloud albedo effect, leading to relatively stronger convection and high cloud formation. The enhanced high clouds increase greenhouse warming and moderate the cooling effect of the low clouds. With respect to the cloud radiative effects, the statistical ST-CLC scheme shows much higher sensitivity to aerosol–cloud coupling for all continental regions than the RH-CLC threshold scheme, most pronounced for low clouds but also for high clouds. Simulations of the short wave cloud radiative effect at the top of the atmosphere in ST-CLC are a factor of 2–8 more sensitive to aerosol coupling than the RH-CLC configurations. The long wave cloud radiative effect responds about a factor of 2 more sensitively.

Our results show that the coupling with the HYB scheme (κ approach) outperforms the coupling with STN (osmotic coefficient), and also provides a more straightforward

ACPD
14, 21975–22043, 2014

approach to account for physicochemical effects on aerosol activation into cloud droplets. Accordingly, the sensitivity of CCN activation to chemical composition is highest in HYB. Overall, the prognostic schemes of cloud cover and cloud droplet formation help improve the agreement between model results and observations, and for the ST-CLC scheme it seems to be a necessity.

1 Introduction

Clouds play an important role in climate by impacting the earth radiation budget and the hydrological cycle (IAPSAG, 2007; IPCC, 2007, 2013). The comprehensive understanding of clouds i.e., their distribution, structure and microphysical properties, is prerequisite to model and project future climate. Pollution aerosol–cloud interactions, in particular the cloud albedo or cloud brightening effect, may have a significant impact on climate change. According to IPCC (2013) the global net radiative forcing on climate due to aerosols and their effects on clouds is estimated at -0.9 (-0.1 to 1.9) $\mathrm{W\,m^{-2}}$, which can vary highly on a regional scale. Compared to the previous report of IPCC (2007), this estimate as well as the uncertainty range have increased, and remain to be the largest contributor to the total uncertainty of anthropogenic radiative forcing.

Clouds are influenced by aerosols that act as cloud condensation nuclei (CCN). Their influences on cloud properties are generally known as aerosol indirect effects (AIE). An increase in available CCN can lead to smaller and more cloud droplets and a more homogeneous size spectrum. These cloud droplets reflect more solar radiation by increasing the cloud optical thickness (cloud albedo effect or Twomey effect or first aerosol indirect effect) (e.g., Twomey, 1977; Kaufman and Fraser, 1997; Han et al., 1998; Reid et al., 1999; Peng and Lohmann, 2003; Schwartz et al., 2002; Feingold et al., 2003). An increased number of smaller and more homogeneous cloud droplets reduces collision and coalescence and thereby the efficiency of precipitation formation (e.g., Rosenfeld, 2000; Penner et al., 2004; Andreae and Rosenfeld, 2008). This can locally suppress precipitation, prolong cloud lifetime and extend cloud top height.

ACPD
14, 21975–22043, 2014

This cloud lifetime effect is also known as the Albrecht effect or second aerosol indirect effect (e.g., Albrecht, 1989; Quaas et al., 2004; Small et al., 2009, Koren et al., 2008; Devasthale et al., 2005; Stevens and Feingold, 2009). The uptake of absorbing aerosol (e.g., soot) in cloud droplets may lead to the increased solar radiation absorption and consequent evaporation, reducing cloud lifetime, i.e., the semi-direct aerosol effect (Ackerman et al., 2000).

The AIE induced changes of cloud reflective properties show a strong regional dependency also related to the properties of the activated aerosols. The aerosol activation is controlled by the size, number and composition of the particles at cloud base and the meteorological conditions. In recent studies the aerosol effects on clouds have been analyzed by satellite observations and also by multi-model simulations. The total AIE is generally regarded to have a cooling effect at the Earth surface (e.g., Lohmann and Feichter, 2005; Penner at al., 2003, 2004, 2006; Lohmann et al., 2007, 2010; Rotstayn et al., 2007; Posselt and Lohmann, 2008; Quaas et al., 2009). It is estimated at about $-1.0\,\mathrm{W\,m^{-2}}$ (Anderson et al., 2003; Lohmann and Feichter, 2005; Forster et al., 2007; Quaas et al., 2008; IPCC, 2013), moderating global warming by increasing greenhouse gas concentrations.

Many modeling studies have emphasized the importance of a realistic description of cloud structure and microphysics for viable climate simulations. Cess et al. (1990, 1996) compared the climate sensitivity of 19 atmospheric general circulation models (GCMs) and identified that the most important differences are mainly attributed to various cloud parameterizations and uncertainties in the representation of aerosol–cloud-interactions. Some of the differences and discrepancies in the estimates of AIEs using GCMs were related to simplified parameterizations based on empirical relations that are restricted to regional or case study observations. As discussed in previous work (e.g., Jones et al., 1994; Lohmann and Lesins, 2003; Anderson et al., 2003), such parameterizations of cloud droplet formation might overestimate the aerosol cooling effect. These approaches are limited in that they do not consider the aerosol size distribution and neglect the aerosol chemical composition effect on aerosol hygroscopic

ACPD
14, 21975–22043, 2014

growth and activation by using single solute particles (e.g., sulfate) as a surrogate for atmospheric aerosols (Jones et al., 1994; Boucher and Lohmann, 1995; Gultepe and Isaac, 1996; Jones and Slingo, 1996; Feichter et al., 1997; Lohmann and Feichter, 1997; Menon et al., 2002; Lance et al., 2004).

More recent attempts to simulate cloud properties including droplet nucleation processes have been more realistic in that they use physically-based parameters such as the aerosol size distribution, composition and vertical velocity. To describe aerosol-cloud interactions, the Köhler equation is widely applied in experimental and theoretical studies of aerosol–cloud interactions. This equation explains the water activity and hygroscopic growth of aerosol up to the supersaturation of water vapor (and relative humidity (RH)) by using curvature and solute effects of aerosol particles (Seinfeld and Pandis, 1998; Pruppacher and Klett, 2000; McFiggans et al., 2006). The various Köhler implementations ranging from parcel models (single column) to global models in many studies can explicitly or analytically calculate the cloud droplet number concentration via parameterizations that account for the aerosol size distribution and solute effects (Hänel, 1987; Ghan et al., 1993, 1995, 1997; Abdul-Razzak et al., 1998; Feingold and Heymsfield, 1992; Chuang and Penner, 1995; Lohmann et al., 1999; Cohard et al., 2000; Abdul-Razzak and Ghan, 2000, 2002, 2004; Nenes and Seinfeld, 2003; Fountoukis and Nenes, 2005; Ming et al., 2006; Khvorostyanov and Curry, 2009; Shipway and Abel, 2010; Wang and Penner, 2009).

Between these studies disagreement could arise from quantifying the solute effect of aerosols by using different approaches, e.g., activity parameterization, osmotic coefficient, Van't Hoff factor models, effective hygroscopicity parameter and analytical approximations. As discussed by Rose et al. (2008), even for relatively simple and well-characterized aerosol composition (e.g., $(NH_4)_2SO_4$, NaCl) discrepancies among the estimated solute effects are substantial. According to Pöschl et al. (2009), depending on the parameterization of the hygroscopic properties, the model results may be associated with about 20 % uncertainty, even though the aerosol chemical composition is regarded as having a minor impact compared to those by other properties (e.g.,

ACPD
14, 21975–22043, 2014

the number and size distribution of particles, transport processes, and the atmospheric ambient conditions) on large scale cloud formation. Particularly for low water vapor supersaturations, low aerosol number concentrations and for organic components, the account of physiochemical aerosol properties is significant (McFiggans et al., 2006; Rose et al., 2008, 2010; and Kreidenweis et al., 2009). For example, aerosol size has been considered to exert a dominant effect on the droplet nucleation process (Dusek et al., 2006; Andreae and Rosenfeld, 2008). Nevertheless, to fully describe aerosol–cloud interactions, more detailed consideration of aerosol composition and hygroscopicity is required for the parameterization of cloud formation.

The κ-method has been introduced to describe the aerosol composition effect on hygroscopic growth that uses the effective hygroscopicity parameter κ based on a model for water activity by Petters and Kreidenweis (2007). It has been investigated by field studies and laboratory experiments to represent the aerosol chemical composition or the CCN activity of aerosols on cloud-nucleating processes (Petters and Kreidenweis, 2007; Snider and Petters, 2008; Wang et al., 2008; Gunthe et al., 2009; Bougiatioti et al., 2009; Rose et al., 2008, 2010, 2011; Niedermeier et al., 2008; Mikhailov et al., 2009; Wex et al., 2009; Dusek et al., 2010; Henning et al., 2010; Shinozuka et al., 2010; Snider et al., 2010; Moore et al., 2012). The κ-method has also been applied in numerical models to calculate the CCN activation of specific aerosol compounds, or certain sizes of aerosols under controlled conditions (Kim et al., 2008; Spracklen et al., 2008; Ruehl et al., 2009; Reutter et al., 2009; Kazil et al., 2010; Su et al., 2010; Pringle et al., 2010b).

The κ parameterization is favored to represent the effect of aerosol chemical composition and hygroscopicity on cloud formation in models because it is flexible in extending the number of aerosol chemical components without explicitly calculating the density, molecular mass and dissociation number of each individual species, e.g., by Van't Hoff factor or osmotic coefficient models (Petters and Kreidenweis et al., 2007; Pöschl et al., 2009; Pringle et al., 2010b). The calculated κ appears to be realistic when compared to measurement-based variables (Gunthe et al., 2009; Rose et al., 2010). By using κ,

ACPD
14, 21975–22043, 2014

the calculation of cloud formation is also numerically effective and robust in calculating solute effects (Pöschl et al., 2009).

Despite the advantages of using κ, there has been no attempt yet to extensively use it for all size modes of aerosols in the calculation of the cloud droplet formation in GCMs. In this study, we apply the κ-method (Petters and Kreidenweis, 2007) to calculate Raoult effects in the Köhler model based on the ARG scheme (Abdul-Razzak and Ghan, 2000). This approach considers aerosol chemical composition effects on the aerosol activation process in a straightforward way. This study shows the sensitivity of the simulated clouds and climate to the Raoult effect (the solute effect) by using different parameterizations. We use two different parameterizations for aerosol activation in the ARG scheme: the original osmotic coefficient approach (standard, STN) and the κ-method (hybrid, HYB). Simulating cloud formation involves a series of integrated processes from activated aerosol to predicted cloud fraction that relate cloud microphysics (aerosol activation parameterization) to macro-scale physics (cloud cover scheme). Furthermore, to address how sensitively different large-scale cloud cover schemes respond to aerosol–cloud coupling based on differing aerosol activation parameterizations, we combine ARG (STN, HYB) with two different large-scale cloud cover (CLC) schemes, i.e., a relative humidity based method (RH-CLC, Sundqvist et al., 1989) and a statistical cloud cover scheme (ST-CLC, Tompkins, 2002). To improve aerosol–cloud coupling for both CLC schemes, a double moment cloud microphysics parameterization (Lohmann et al., 2007) is applied that distributes cloud droplets by number and size, to represent the feedbacks between aerosols, clouds and climate.

In the following sections we describe the treatment of cloud droplet nucleation in the EMAC atmospheric chemistry-climate model, and show the sensitivity of simulated clouds to different formulations, including the cloud radiative responses to aerosols and CCN activation. The sensitivity simulations are inter-compared and evaluated on the basis of satellite observations by the Moderate Resolution Imaging Spectroradiometer (MODIS), International Satellite Cloud Climatology Project (ISCCP), Clouds and the Earth's Radiant Energy System (CERES), A-Train (Aqua, Aura, CloudSat and

ACPD
14, 21975–22043, 2014

CALIPSO satellites) multi-year mean data, and the global precipitation climatologies of the Global Precipitation Climate Project (GPCP).

2 Model description

2.1 EMAC Atmospheric Chemistry-Climate model

We used the ECHAM5-MESSy Atmospheric Chemistry-Climate model (EMAC) to simulate cloud distributions and characteristics, including radiative properties and climatically relevant parameters. EMAC is a numerical chemistry and climate model based on the general circulation model ECHAM5 (Roeckner et al., 2006, version 5.3.01), combined with the Modular Earth Sub-model System (MESSy version 1.10, Jöckel et al., 2005, 2006). A full description of EMAC and its evaluation are documented in Jöckel et al. (2005, 2006); Pozzer et al. (2010, 2012); Pringle et al. (2010a); de Meij et al. (2012), see also http://www.messy-interface.org. The present study uses the T42L19 resolution corresponding to a gaussian grid of approximate 2.8° by 2.8° in latitude and longitude with 19 vertical hybrid pressure levels up to 10 hPa and a time step of 30 min, and comprises the submodels summarized in Table 1. A schematic flow diagram of aerosol, cloud and climate coupling is presented in Fig. 1.

2.2 Atmospheric aerosol (GMXe)

The aerosol submodel GMXe (Pringle et al., 2010a) is coupled with the cloud droplet formation process to feed the computed aerosol size and number distributions and chemical composition back onto the cloud droplet and the cloud ice crystal size distribution. GMXe simulates aerosols with lognormal distributions in seven interacting modes, i.e., four soluble ones (nucleation, Aitken, accumulation and coarse mode) and

ACPD
14, 21975–22043, 2014

three insoluble ones (Aitken, accumulation and coarse mode):

$$n(\ln a_r) = \sum_{i=1}^{7} \frac{N_i}{\sqrt{2\pi}\ln\sigma_i} \exp\left(-\frac{(\ln a_{r,i} - \ln \overline{a}_{r,i})^2}{2\ln^2\sigma_i}\right) \quad (1)$$

where each aerosol mode (i) is described with the number concentration (N_i), the mean radius ($\overline{a}_{r,i}$) and the standard deviation (σ_i). These variables are summarized in Table 2. Aerosol number and mass are prognostically calculated (i.e., subject to transport, microphysics and chemistry), whereas σ_i is prescribed for each aerosol mode (σ = 2.0 for the coarse mode, σ = 1.59 for the other modes) and the mean mode radius is diagnosed every time step. The overlap of a lognormal distribution with neighboring modes defines the cross mode exchange.

The chemistry calculations distinguish between soluble and insoluble modes, and each mode is assumed to be internally mixed. The version of GMXe used here treats bulk species (no specification of internal composition, e.g., black carbon (BC), particulate organic matter (POM, also organic carbon, OC), dust (DU) and sea spray (SS)), in addition to aerosols with detailed chemical specifications (e.g., SO_4^{2-}, H_2SO_4, HSO_4^-, NO_3^-, NH_4^+, Na^+, Cl^-). This is a compromise between speciated chemical species and bulk species, and the latter can be extended with specific chemical components. This has been evaluated by Pringle et al. (2010a) in the comparison between the simulated aerosol field and observations. The aerosol fields are also comparable to the AeroCom global models (Mann et al., 2014) and ECHAM-HAM (Stier et al., 2005). The water uptake is diagnosed for each type at every time step. GMXe also calculates the effective hygroscopicity parameter κ and the supersaturation in each aerosol mode based on the κ-Köhler theory. These variables determine the CCN activity in the cloud droplet nucleating process. The global distribution of κ in EMAC has been presented in Pringle et al. (2010b), where κ was diagnosed from the aerosol distribution but did not interact with clouds.

ACPD
14, 21975–22043, 2014

2.3 Cloud droplet nucleation (CDN)

A CDN parameterization scheme (hereafter, standard STN) was developed by Abdul-Razzak et al. (1998) and Abdul-Razzak and Ghan (2000), and implemented in EMAC with explicit aerosol coupling. It describes the formation of cloud droplets by condensation and the subsequent growth of cloud droplets relying on aerosol physicochemical properties (e.g., size distribution, mass and number concentrations and chemical composition) based on the hygroscopic growth of particles through Köhler theory. The performance of this parameterization (STN) has been presented and discussed for a mono-modal single-solute aerosol in Abdul-Razzak et al. (1998) and for a multi-modal multi-solute aerosol distribution in Abdul-Razzak and Ghan (2000, 2002).

The hybrid CDN parameterization (hereafter, HYB) replaces the calculation of the critical supersaturation in STN, which is based on an osmotic coefficient model, with the κ method, see Fig. 1 and Table 3 for a summary. As shown in Table 3, the critical saturation in HYB ($s_{c_\kappa} = S_{C_\kappa} + 1$) for a dry diameter ($D$) is defined by the water activity in the aqueous solution droplet (a_w), and the curvature effect (or Kelvin effect, denoted by A). The surface tension of the pure water ($0.072\,J\,m^{-2}$) is used for the calculation of A and s_{c_κ} in HYB (Petters and Kreidenweis, 2007; Gunthe et al., 2009; Pöschl et al., 2009; Rose et al., 2010; Pringle et al., 2010b). The a_w can be expressed in terms of the solute effect that describes aerosol composition and the effective hygroscopicity parameter. In each aerosol mode the multi-solute κ_i is obtained from the volume weighted mean of the single solute $\kappa_{i,j}$. The κ_j values are mainly from Petters and Kreidenweis (2007); 0.61 for $(NH_4)_2SO_4$, 0.67 for NH_4NO_3, 1.28 for NaCl, 0.90 for H_2SO_4, 0.88 for $NaNO_3$, 0.91 for $NaHSO_4$, 0.80 for Na_2SO_4, and 0.65 for $(NH_4)_3H(SO_4)_2$; 0.0 for black carbon (BC) and 0.1 for organic carbon (OC) (Wang et al., 2008; Gunthe et al., 2009; Pöschl et al., 2009; Dusek et al., 2010; and Pringle et al., 2010b); for dust $\kappa_{DU} = 0.03$ is recommend as a global mean value (Koehler et al., 2009). The calculated κ_i values have been evaluated for several compositions by measurements (Gunthe et al., 2009; Rose et al., 2010).

ACPD
14, 21975–22043, 2014

The calculated S_{C_κ} is applied to the parameterization of the water condensation rate (dw/dt) of the activated droplets in STN and the hygroscopic growth is then defined by

$$\frac{dw}{dt} = 4\pi\rho_w \sum_{i=1}^{7} \int_0^S r_i^2 \frac{dr_i}{dt} \frac{dn_i(S_C)}{da} dS_C \quad (2)$$

where $n_i(S_C)dS_C$ is the number concentration of particles activated between S_C and $S_C + dS_C$ and r_i is the radius of the forming droplet in aerosol mode (i) during the changes of aerosol (da) and over time (dt). A detailed derivation and solution of the equation are described in Abdul-Razzak et al. (1998) and Abdul-Razzak and Ghan (2000).

Both STN and HYB calculate the nucleation cloud droplet number concentration based on the physicochemical aerosol properties. HYB uses the κ-Köhler method to estimate the Raoult effect on the CCN activity and hygroscopicity that can efficiently calculate the rate of nucleation of cloud droplets (R_{nuc}) without the need of specific aerosol information (e.g., osmotic coefficient and dissociation number of each chemical component) in STN.

By coupling the aerosol submodel GMXe to the cloud module, the ice crystal number concentration (N_i) is also influenced by the semi-speciated soluble aerosol species (i.e., SO_4^{2-}, H_2SO_4, HSO_4^-, NO_3^-, NH_4^+, Na^+, Cl^-). This affects the calculation of contact freezing of hydrophobic aerosols that act as ice nuclei (IN, e.g., DU, BC) and the immersion freezing of solute aerosols through heterogenous freezing.

2.4 Cloud microphysics (CLOUD)

The nucleated droplets from the ambient aerosols in large-scale clouds (hence not the distinctly parameterized convective clouds) represent aerosol–cloud interactions in this study. For the representation of these interactions the aerosol sub-model GMXe is coupled with the cloud microphysics to describe the influence of ambient aerosol size

ACPD
14, 21975–22043, 2014

distributions and chemical composition on the cloud droplet and ice crystal forming processes. The nucleation processes represent AIEs and occur only at cloud base. The calculated cloud properties are based on a double moment cloud microphysics scheme that accounts for cloud droplet size and number distribution.

The changes in the total number of cloud droplets (CDNC) $\frac{dN_d}{dt}$ and cloud ice crystals (ICNC) $\frac{dN_i}{dt}$ are calculated from individual cloud microphysical processes. This has been described in detail and discussed in Lohmann et al. (1999); Lohmann (2002, 2007); and Hoose et al. (2007):

$$\frac{dN_d}{dt} = \left[\frac{N_d}{dt}\right]_{transport} + R_{nuc} + R_{melt} - R_{auto} - R_{self} - R_{acc} - R_{frz} - R_{evap} \quad (3)$$

$$\frac{dN_i}{dt} = \left[\frac{N_i}{dt}\right]_{transport} + R_{nuc,i} + R_{frz} + R_{secp} - R_{agg} - R_{self,i} - R_{acc,i} - R_{melt} - R_{sub} \quad (4)$$

The first terms on the right-hand sides ($[\frac{N_d}{dt}]_{transport}$ and $[\frac{N_i}{dt}]_{transport}$) denote the rate of change in cloud droplet and in ice-crystal numbers by all transport processes including advection, convection and diffusion. The subsequent R terms represent the rate of change in cloud droplet number by nucleation, melting, autoconversion (rain droplets), self-collection, accretion (falling rain or snow), heterogeneous freezing (contact and immersion) and evaporation (R_{nuc}, R_{melt}, R_{auto}, R_{self}, R_{acc}, R_{frz}, R_{evap}, respectively).

The rate of change in ice-crystal number is obtained from homogenous nucleation $R_{nuc,i}$ (below −35 °C), heterogenous freezing R_{frz} (between 0 and −35 °C), secondary production, aggregation (snow), self-collection, accretion (falling snow) and by sublimation (R_{secp}, R_{agg} $R_{self,i}$, $R_{acc,i}$ and R_{sub}, respectively). All soluble aerosol particles (exception the nucleation mode) are assumed to be supercooled below −35 °C and homogeneously frozen, potentially forming cloud ice crystals. Note that also chemically aged dust and BC can take a part in homogenous ice crystal formation. The heterogenous freezing of cloud droplet is treated by two processes; contact freezing for insoluble particles, i.e., dust and BC, and immersion freezing for soluble particles including aged

ACPD
14, 21975–22043, 2014

dust and BC. For details see the original work (Kärcher and Lohmann, 2002; Lohmann et al., 2007; Hoose et al., 2008) which has been extended accordingly to consider the more comprehensive aerosol composition and size and number distribution of GMXe (Pringle et al., 2010).

R_{auto} is parameterized according to Kharioudinov and Kogan (2000) and calculates the total cloud mass and number distribution by changes in the cloud water content by forming precipitation as well as R_{agg}. It can be understood as a relevant parameter of the second AIE, i.e., the cloud lifetime effect (Tompkins, 2002; Lohmann et al., 2007; Pincus et al., 2008; Reichler and Kim, 2008). The self-collection terms (R_{self} and $R_{self,i}$) also influence the cloud particle size distribution but do not change the total mass of cloud water. The relevant variables for nucleation, evaporation and sublimation (i.e., in the calculation of $R_{nuc}, R_{nuc,i}, R_{evap}, R_{sub}$) are diagnosed at each time step. These variables are used for the calculation of cloud cover, and the new total tendencies of cloud droplet number concentration (CDNC) and ice crystal number concentration (ICNC). The updated CDNC and ICNC values are used for the calculation of radiation in the next time step.

The CDNC in the REF-simulations is prescribed by a pressure dependent function which is basically the product of surface concentration (distinct for land and ocean) and a term that exponentially decreases with pressure. Note that no explicit aerosol–cloud interactions are included in the convection parameterization.

2.5 Large-scale cloud cover

EMAC has two cloud cover schemes to simulate large-scale cloud cover, i.e., the relative humidity (RH) dependent scheme (Sundqvist et al., 1989, hereafter, RH-CLC) and the statistical cloud cover (ST) scheme (Tompkins, 2002, hereafter, ST-CLC). RH-CLC defines fractional cloudiness with variances of humidity in a gridbox using a tunable value depending on the size of a gridbox, and simulated clouds are consequently influenced by model height and resolution. ST-CLC determines cloud fraction with a

ACPD
14, 21975–22043, 2014

parameterization of variable water vapor and cloud condensate at the sub-grid scale of clouds using a probability density function (Tompkins, 2002).

2.6 Experimental design

All simulations are based on identical meteorological boundary conditions. The distributions of aerosol particles and cloud properties are generated as integrated long term simulations with climatological sea surface temperature (SST) and sea-ice (SIC) to perform the statistical analysis of free-running simulations. Therefore, feedbacks of changing cloudiness on the surface energy budget and evaporation, and influences on the dynamics and convection are suppressed over the oceans (fixed SSTs) whereas such effects are allowed over the continents. The year 2000 is used for aerosol emissions and repeated for all simulation periods. Emission fields of aerosols are based on AEROCOM (an AEROsol module inter-COMparison in global models) (Dentener et al., 2006), also used by Pringle et al. (2010a).

We have summarized the different model setups in Table 4. Apart from the reference runs all simulations applied prognostic CDN parameterizations (i.e., STN and HYB) and have been performed for 10 year periods after an initial spin-up of 1 year. The reference simulations (i.e., RH-REF and ST-REF) have been conducted for 5 years after 1 year spin-up time.

The simulations have been performed with the following objectives: (1) to better understand the effects of aerosol–cloud interactions by comparing the REF-simulations to the simulations that apply the prognostic CDN parameterizations (STN, HYB), (2) to investigate the influence of aerosol chemical composition effects on the formation of large scale clouds based on the comparison between the STN and HYB simulations, and (3) to examine the impact of the cloud cover scheme on the simulated cloud properties and climate relevant parameters via the inter-comparison of all simulations applying RH-CLC and ST-CLC. The analysis focuses on cloud and climate relevant properties that can be compared to global scale observations.

ACPD
14, 21975–22043, 2014

The performance of EMAC in simulating cloud properties is assessed based on the following multi-year data sets, being averaged over the available time period; for cloud properties the Moderate Resolution Imaging Spectroradiometer (MODIS), International Satellite Cloud Climatology Project (ISCCP), Clouds and the Earth's Radiant Energy System (CERES), and A-Train (Aqua, Aura, CloudSat and CALIPSO satellites); for the cloud radiative forcing at TOA the CERES Energy Balanced And Filled (EBAF); for the aerosol optical properties MODIS; and for the global precipitation climatologies the Global Precipitation Climate Project (GPCP).

3 Model results

3.1 Annual global mean values

An overview of the global mean cloud properties, radiation and water budgets is given in Table 5 for the simulations and observational data.

The multiyear global mean liquid water path (LWP) ranges from 30 to 50 g m^{-2} according to recent observations of A-Train satellites (based on MODIS Aqua (October 2002 to September 2008) and CloudSat (August 2006 to July 2010); Jiang et al., 2012). Another observational estimate of LWP from CERES Terra SYN1deg between March 2000 and February 2010 is about 38 g m^{-2}. For the reference simulations, RH-REF agrees well with the observations, while ST-REF is clearly too low. The LWP in the STN-simulations (i.e., RH-STN and ST-STN) is overestimated (93.2 and 75.4 g m^{-2}). In the HYB simulations, LWP in RH-HYB is 20 % higher than the upper range value of observations, and LWP in ST-HYB fits well within the range of observations.

Ice water path (IWP) from ISCCP, CloudSat and MODIS observations ranges from 24 to 70 g m^{-2} as the best estimate (Jiang et al., 2012). The IWP from the observational data has a relatively large spread, larger than that of LWP. The simulated IWP appears to be rather more sensitive to the cloud cover scheme (RH-CLC and ST-CLC) than to

ACPD
14, 21975–22043, 2014

aerosol–cloud coupling. The RH-simulations tend to estimate about 24 % higher values than the ST-simulations. Overall, the predicted IWP in all simulations is in agreement with the observations though in the lower part of the range.

The calculation of the vertically integrated cloud droplet number concentration (N_d) shows large sensitivity to aerosol–cloud coupling (i.e., the prognostic CDN parameterizations) as well as the simulated LWP. In the STN-simulations, the calculated N_d is more than twice that of N_d in the HYB-simulations. As mentioned above, the REF-simulations do not include the nucleated cloud droplets from the aerosol–cloud interaction, and diagnostically calculate relatively small values compared to the other simulations. The estimated N_d is compared with the observed global annual mean N_d of $4.0 \times 10^{10}\,\mathrm{m}^{-2}$ based on the ISCCP data between 50° N and 50° S during four months (January, April, July, October in 1987) representing four seasons (Han et al., 1998). The HYB-simulations predict cloud droplet number concentrations rather well, particularly with RH-CLC (i.e., RH-HYB). While the STN-simulations strongly overestimate the droplet number concentrations, the differences among the CLC schemes are small. The calculated vertically integrated ice crystal number concentrations (N_i) do not show strong differences between the simulations based on the global annual mean values.

The global annual mean of total water vapor mass (WVM) is estimated at 24.7 and $23\,\mathrm{kg\,m}^{-2}$ from the multiyear mean of CERES Terra (Wielicki et al., 1996) from MODIS Terra for 10 years, and A-Train satellite observations from AIRS (October 2002 to September 2010) + MLS (September 2004 to August 2011), respectively. The predicted WVM in all simulations shows little sensitivity to different cloud parameterizations and is slightly higher compared to the observed WVM. The global mean from CERES observations is based on the regridded data (matched with a horizontal resolution T42) and area-weighted average in this study. This may lead to slightly different values compared to literature reports. This also applies to the other observed data, e.g., total cloud cover, total precipitation, cloud radiative effect and aerosol optical depth.

The multiyear mean total cloud cover (TCC) is around 66 % as derived from Terra and Aqua MODIS and ISCCP data. Generally, the RH-simulations slightly overestimate

ACPD
14, 21975–22043, 2014

TCC by 5 %, whereas the ST-simulations underestimate TCC by up to 15 % compared to the observations. The simulations with RH-CLC are less sensitive to the changes in cloud droplet distribution and aerosol–cloud coupling compared to the simulations with ST-CLC. The clouds simulated by ST-CLC are more sensitive to the representation of cloud properties such as cloud water and droplet number concentration. Discrepancies of total cloud cover computed with RH-CLC and ST-CLC might become smaller with higher model resolution, which reduces the degree of subgrid parameterization dependent on the humidity variance (Tompkins, 2005).

Total precipitation (P_{total}) is estimated from the Global Precipitation Climatology Project (GPCP) long-term monthly means, derived over the years 1981 to 2010 (Adler et al., 2003). All EMAC simulations slightly overestimate P_{total} by about 10 % compared to the estimate of GPCP (2.68 mm day^{-1}). There are no significant differences between the simulations due to the fact that precipitation is largely controlled by evaporation from the oceans with prescribed SST and SIC. These constrained ocean temperatures suppress the changes in total precipitation but some differences occur nevertheless. The large scale precipitation decreases in favor of convective rainfall due to increases in small cloud droplets, being less efficient to form rain, particularly in the STN-simulations that generate a relatively large number of cloud droplets. This affects precipitation over the continents, but does not show in the annual global mean values.

The cloud radiative effect (CRE) is defined as the difference between the radiation fluxes for cloudy and cloud-free regions (i.e., all sky – clear sky). At the top of the atmosphere (TOA), the shortwave cloud radiative effect (SCRE) is estimated at about $-47.2\,\mathrm{W\,m^{-2}}$ and the longwave radiative effect (LCRE) at about $26.3\,\mathrm{W\,m^{-2}}$ based on the Clouds and the Earth's Radiant system experiments, Energy Balanced and Filled data (CERES EBAF) from 2000 to 2010 (Loeb et al., 2009). In view of the regional uncertainties in the SW and LW fluxes, the reported ranges are -43.2 to $-51.2\,\mathrm{W\,m^{-2}}$ for the SW, and 23.8 to 28.8 $\mathrm{W\,m^{-2}}$ for the LW (CERES EBAF Edition2.6r Data Quality Summary).

ACPD
14, 21975–22043, 2014

Depending on the cloud cover schemes a general tendency of the CREs in the simulations is apparent; both the SCRE and LCRE in the RH-simulations are larger than in the ST-simulations. In particular the SCRE is strongly influenced by the cloud droplet number concentration. This is reflected in the enhanced SCRE in the simulations that applied aerosol–cloud coupling. The SCRE in ST-REF is underestimated by $-9.4\,W\,m^{-2}$ (29 %) compared to the observations. This bias reduces substantially by including aerosol–cloud feedback, i.e., the mean difference with the observations reduces to $-4.9\,W\,m^{-2}$ (about 10 %) for ST-STN and $8.3\,W\,m^{-2}$ (about −18 %) for ST-HYB. For the RH-simulations, the difference with the observations is increased with aerosol–cloud coupling, only slightly with HYB and strongly with STN. Overall the estimates of SCRE in ST-STN, ST-HYB and RH-REF are relatively close to the observational range, while the LCRE in all simulations is within the observed range. The predicted net cloud radiative effect (NCRE) at the TOA in ST-HYB and ST-STN are in fair agreement with the estimated NCRE from CERES EBAF, though with different signs of the biases.

The calculated aerosol optical depth (AOD) in all EMAC simulations is overestimated compared to the multiyear mean of AOD obtained from the combined data of Terra and Aqua in MODIS over 10 years of observations. Note that this is also improved in higher resolution simulations (de Meij et al., 2012). Estimated AODs in the ST-simulations are within the observed uncertainty range (Stier et al., 2005) except ST-STN. In general, the simulations considering aerosol–cloud feedback predict higher AOD than the REF-simulations, indicating that the presence of aerosols decreases the efficiency by which they are removed through precipitation. The estimated AODs in the RH-simulations are higher by about 10 % compared to the ST-simulations.

3.2 Zonal distribution of cloud properties and energy budget

Annual zonal mean cloud properties, water budgets and cloud radiative effects are presented in Figs. 2–4 for the simulations and observational data.

ACPD
14, 21975–22043, 2014

The zonal mean distributions of vertically integrated cloud droplet numbers (N_d) are strongly dependent on the droplet nucleation parameterizations as shown in Fig. 2. Both prognostic CDN (STN and HYB) simulations produce higher CDNC compared to the REF-simulations with prescribed aerosol distributions for the cloud droplet nucleation process. These differences also appear in the annual global mean values, see Table 5. The STN-simulations yield larger numbers of cloud droplets compared to the HYB-simulations. As can be seen from Fig. 6 for the cases ST-STN vs. ST-HYB, the largest differences are associated with continental clouds. The strongest effect appears in the tropics and the Northern Hemisphere (NH) in Fig. 2, with high aerosol concentration over the continents. The zonal mean distributions of the vertically integrated ice crystal numbers (N_i) show only weak sensitivity to the aerosol–cloud coupling, predominantly in mid-latitudes of the NH for the statistical cloud cover scheme.

As shown in Fig. 3, the distributions of liquid water path (LWP) show large discrepancies and are significantly sensitive to the treatment of aerosol–cloud feedback and the choice of cloud cover scheme. The LWP increases rapidly with increasing CDNC (Fig. 2) for both CLC schemes. Furthermore only the ST-CLC reproduces the observed zonal LWP distribution with a distinct minimum in the tropics and maxima in mid-latitudes. Actually the ST-HYB outperforms by far the other model configurations in reproducing the CERES-Terra observations, in line with the results obtained for SCRE in Table 5. It clearly simulates the most realistic meridional profiles and magnitudes of LWP, especially between 35° S and 70° N. The STN-simulations tend to produce large LWP with both CLC-schemes reflecting the large number of CDNC shown in Fig. 2. This seems more important for radiative forcing than for precipitation.

The zonal distributions of ice water path (IWP) generally show a stronger response to the cloud cover schemes than to aerosol–cloud coupling, except for northern mid-latitudes where anthropogenic aerosols are most abundant. Over these latitudes, differences appear related to the heterogenous freezing process as it is a part of the aerosol–cloud coupling effects. The difference in ICNC of Fig. 2 results in an increased spread in IWP.

ACPD
14, 21975–22043, 2014

The zonal distributions of total water vapor mass (WVM) in all simulations do not vary much among the different set-ups, and are close to the observations. For the annual zonal mean distribution of precipitation all EMAC simulations show similar meridional profiles with the well captured double peaks at 10° N and 10° S over the tropics, in both hemispheres in generally good agreement with the observations (GPCP). The simulated precipitation shows less sensitivity to the aerosol–cloud interactions due to the current model setup using a fixed SST and SIC and therefore constraining total evaporation and precipitation. Nevertheless, the midlatitude maximum in the Southern Hemisphere (SH) shows some sensitivity to the parameterization of warm cloud formation. Compared to observations, the model overestimates precipitation at lower latitudes between 0 and 10° S. These discrepancies may to some degree relate to the coarse model resolution. According to Hagemann et al. (2006), the model resolution could influence the hydrological cycle in the ECHAM5 model; by increasing vertical resolution, total and large-scale precipitation are systematically increased and convective precipitation is decreased, particularly over the indicated regions (between 0 to 10° S). This may lead to overestimated convective precipitation in the L19 simulations, probably being more realistic in the L31 simulations. It has also been suggested by Roeckner et al. (2006) that atmospheric dynamics and thermodynamics are substantially improved at higher vertical resolution (L31) but only in combination with higher horizontal resolution (T63 and higher), but for T42 the resolution L19 is generally the better choice (Roeckner et al., 2006).

As shown in Fig. 4, the zonal mean distributions of total cloud cover (TCC) demonstrate notable differences between the simulations and the observations especially at high latitudes. The latter could partly be caused by systematic deficiencies of the satellite retrievals rather than model error over the bright surfaces such as desert areas and snow or ice regions. By excluding the polar regions estimated TCC by RH-CLC shows good agreement with MODIS and ISCCP at the middle and higher latitudes and in general between 60° S and 60° N, while the simulated TCC by ST-CLC is underestimated. The estimated TCC by RH-CLC indicates a larger cloud fraction and is less sensitive

ACPD
14, 21975–22043, 2014

to changes induced by aerosol–cloud coupling. Different cloud patterns related to the cloud cover schemes occur in all latitudes and in both hemispheres, whereas the sensitivity to aerosol–cloud coupling is strongest from 30° S to the north pole.

The aerosol optical depth (AOD) in the simulations varies latitudinally with peaks at 50–60° in the SH and the subtropics and midlatitudes in the NH. Compared to the observations (MODIS) the patterns of simulated AOD match relatively well, but the magnitudes of simulated AOD are generally overestimated, particularly in the SH. These discrepancies are related by the over-predicted AOD over the ocean being mainly determined by sea spray as discussed in Pringle et al. (2010a). Too high aerosol mass burdens (AEROCOM emission data are used) and/or parameterizations of aerosol size and number distribution may further contribute to overestimated AOD. A further study involving a sensitivity test with various parameters determining the aerosol number and size distribution would be worthwhile, but is not the focus here. Some of the differences could also be associated with uncertainty in the MODIS AOD data. According to some data quality studies, the expected MODIS AOD error ($\Delta\tau_{550\,\mathrm{nm}}$) is estimated as $\pm(0.03 + 0.05\tau_{550\,\mathrm{nm}})$ over ocean (Kaufmann et al., 1997; Tanré et al., 1997) and $\pm(0.05 + 0.15\tau_{550\,\mathrm{nm}})$ over land (Chu et al., 2002; Levy et al., 2010; Yoon et al., 2014).

The zonal mean distributions of SCRE and LCRE are shown in Fig. 4. The differences in cloud radiative effects are more significant for the zonal distribution of SCRE than LCRE in all simulations. The patterns of LCRE seem more sensitive to the cloud cover scheme than to aerosol–cloud coupling, i.e., the CDN parameterizations, with RH-CLC showing higher LCRE than ST-CLC except at high latitudes where both schemes are very similar. Between 40° S and 50° N RH-CLC is close to the LCRE observations, whereas ST-CLC tends to underestimate LCRE.

The observed zonal mean SCRE shows a typical value of $-45\,\mathrm{W\,m^{-2}}$ in the tropics and subtropics, a distinct maximum of cooling in the high mid-latitudes (more pronounced in the SH), and declining towards the poles (i.e., over bright surfaces and low SW radiation intensity). Generally the simulations resemble this pattern, but with large variability. This and discrepancies with observations are mainly driven by differences in

ACPD
14, 21975–22043, 2014

total cloud cover and liquid water path, i.e., responding to cloud droplet number concentration. Since total cloud cover is more dependent on the choice of the cloud clover scheme, except for very high CDNC, and not so much on aerosol–cloud interactions, the aerosol feedback on LWP (CDNC) is the main driver for the high variability in the predicted SCRE. This is quite obvious for the RH-simulations with almost identical TCC except in high northern latitudes.

The ST-CLC responds differently depending on the simulated CDNC. For ST-HYB the LWP resembles observations, and therefore the difference to observed SCRE is caused by the underestimation of TCC, which does not differ from TCC in ST-REF, in contrast to LWP. Whereas for ST-STN SCRE responds predominantly to the high CDNC. In the NH, SCRE is overestimated due to very high LWP, whereas TCC is close to observations. SCRE in the SH resembles observations, caused by the compensating effect of too low TCC and overestimated LWP. Note that with observed TCC and LWP, e.g., at 55° N for ST-HYB, the radiation code reproduces the observed SCRE and LCRE well.

3.3 CCN activation

The calculation of CCN activation starts with estimating the radius of the smallest activated particle in each aerosol mode. The two cloud droplet nucleation schemes, STN with the osmotic coefficient model and HYB with the κ method, are summarized in Table 3. Subsequently the fractions of activated aerosol (AF_i) are calculated for each mode, which are then used in calculations of cloud microphysics and cloud droplet formation.

3.3.1 Annual global mean

Table 6 presents the global mean values based on volume-weighted averaging from the surface to the upper troposphere (about 10 km). Large particles in the accumulation and coarse modes show higher activities (AF_{Acc} and AF_{Cor}) than small particles in the

ACPD
14, 21975–22043, 2014

Aitken mode (AF_{Atk}) in both the STN- and HYB- simulations. This corroborates that particle size generally dominates over composition in CCN activation (Dusek et al., 2006; Andreae and Rosenfeld, 2008).

The efficiency of CCN activation is strongly influenced by the choice of the supersaturation (Sc) algorithm; the HYB simulations estimate lower AF_i ($\approx 50\,\%$) for all modes compared to the STN simulations. The calculated CCN_{total} in the STN-simulations is more than twice that in the HYB-simulations. These differences are most pronounced in the boundary layer and the lower troposphere (Fig. 5a and b) and do not show a substantial mode dependence with the exception of the tropopause region (Fig. 5c and d), where large aerosols are scarce. Furthermore Table 6 confirms that the choice of the cloud cover scheme is generally of minor importance with the relevant exception of CCN_{Atk}, which is the dominant source for CCN formation in all simulations. The differences in CCN directly propagate into cloud droplet number concentration as can be seen from the comparison of CCN_{total} and CDNC (therefore not shown in Table 6).

In our model setup both size and chemical composition of aerosols have a significant impact on droplet nucleation. According to Köhler theory, larger particles have a lower Sc than smaller particles, since the Kelvin effect decreases with increasing particle size (i.e., smaller surface tension). Furthermore the activation of large aerosols is to a lesser extent dependent on their composition, because the Raoult effect is of less importance when the particles are more diluted. On the other hand, in small particles water uptake relies more on composition since the Raoult effect has to offset the Kelvin effect. This size effect is clearly captured by the simulations, and the accumulation and coarse modes show nearly the same activated aerosol fraction (AF), which is approximately three times that of the Aitken mode. Therefore these differences can be understood as significant sensitivities of the supersaturation algorithms applying different approaches of the solute effect (i.e., the osmotic coefficient and the κ-Köhler method). As discussed by Rose et al. (2008), the difference of the computed solute effect of aerosols (even for simple solutions and well-characterized particles) can be substantial. It has been estimated (Pöschl et al., 2009) that model results of large scale cloud formation could differ

ACPD
14, 21975–22043, 2014

by 20 % depending on the parameterization of aerosol hygroscopicity, even though the chemical composition is regarded as a relatively small influence compared to other variables (e.g., the number and size distributions of particles, transport processes, and atmospheric ambient conditions). However, our simulations suggest a substantial sensitivity up to a factor of two. The importance of chemical (composition) effects is largely related to the fact that the Aitken mode, for which the Raoult effect is highly relevant, is a dominant source of CCN, i.e., number concentration matters (Feingold, 2003) in all simulations (63 % for STN and 71 % for HYB) and all altitudes. Particularly for low water vapor supersaturations, low aerosol concentrations, and the presence of organic components, hence the explicit description of physicochemical aerosol properties is significant (McFiggans et al., 2006; Rose et al., 2008, 2010; Kreidenweis et al., 2009). Please note that anthropogenic emissions have a strong influence on this aerosol size mode.

3.3.2 Vertical profiles of annual global mean

The vertical distribution of the activated aerosol fraction (AF_i) is presented in Fig. 5 for the Aitken, accumulation and coarse modes. The AF_i ranges from 0 to 1, and the modes are added at each vertical level, i.e., the accumulated value spans the range from 0 to 3. Figure 5 only shows the ST-STN and ST-HYB simulations, since RH-STN and RH-HYB yield very similar results (see Supplement Fig. S2).

The total activated fraction in the ST-STN simulation has a distinct L-shape with altitude, with most activation in the lower boundary layer, nearly 1 for $AF_{Acc,\,Cor}$ and 0.7 for AF_{Atk}, and typical values of 0.5 for $AF_{Acc,\,Cor}$ and 0.1 for AF_{Atk} at the top of the boundary layer, in the free troposphere and the tropopause region. The vertical AF distribution in ST-HYB has more of an hourglass shape, which is predominantly caused by a distinct minimum in AF_{Atk} at the boundary layer top and in the lower free troposphere. Generally the total activated fraction in ST-HYB is half to a third that in ST-STN with the exception of higher altitudes, with $AF_{Acc,\,Cor}$ being about 0.3 in the upper troposphere and an AF_{Atk} of 0.25 near the surface, relatively low values at the

ACPD
14, 21975–22043, 2014

boundary layer top and increasing to 0.15 in the upper troposphere and tropopause region.

Apart from the differences in activation in the two simulations, on a global scale ST-STN seems to be more sensitive to the chemical composition of the aerosols. The simulations show large differences in AF_{Atk}, but only ST-STN produces strong changes in $AF_{Acc,\,Cor}$ with height. This is not supported by more detailed analysis. The global hourglass shape in the ST-HYB results from a pronounced hourglass shape over the ocean and a funnel shape over land. In fact, examination of the vertical distribution of aerosol activation for distinct continental regions reveals higher sensitivity of the HYB-simulations to aerosol composition.

The relative differences in activated fractions, separately plotted over the ocean and land in Fig. 5c and d, do not differ much for all modes. There appears to be a pronounced distinction of the relative difference in activated fraction in the PBL, which is 75 % over land and 50 % over the ocean. Hence the two schemes have a different sensitivity in activating marine and continental aerosols. This is confirmed by Fig. 5e and f, which shows the relative difference in activation (ocean–land) for both simulations. As can be seen from Fig. 5e, ST-STN simulates no difference below 2 km in the activated fraction for continental and marine aerosol, whereas ST-HYB calculates a 50 % higher activation for marine aerosols in the lower troposphere, indicating a strong land–sea gradient in the activated fraction. The land sea-gradient in aerosol activation above 2 km is more similar in both simulations, especially for Aitken mode particles, whereas $AF_{Acc,\,Cor}$ in ST-HYB shows a considerably higher activation over land (25 % higher activation) compared to ST-STN (10 %).

In summary, the STN-simulation tends to not sensitively discriminate between continental and marine aerosol activation, except for Aitken mode particles in the free troposphere, and simulates a strong vertical gradient in activated fraction between the boundary layer and free troposphere. This is in contrast to ST-HYB which simulates pronounced land–sea gradients in activated fraction for all modes from surface to tropopause, a less pronounced vertical gradient between the boundary layer and free

ACPD
14, 21975–22043, 2014

troposphere and a much lower total activated fraction in the boundary layer and lower free troposphere. Both simulations corroborate that not only the size is important in droplet formation (i.e., higher activity of larger particles) but that there is also a strong sensitivity to aerosol chemistry in all particle size modes being most pronounced for the Aitken mode. Dusek et al. (2006) demonstrated the distinct sensitivity of CCN activation to the particle chemical composition, even though it was indicated to play a secondary role. The overall largest differences between the two schemes are found for low clouds where the aerosol activation is tightly linked with the cloud optical properties. With high aerosol activation low clouds tend to be relatively optically thick and more strongly reflect the incoming solar radiation thereby exerting a cooling effect on climate.

To understand the aerosol–cloud feedback for specific cases depending on different aerosol compositions, we discuss in the next section selected regions with aerosols in specific conditions, e.g., related to air pollution and natural emissions.

3.3.3 Regional distributions

To examine the geographic sensitivity of aerosol activation in more detail we selected 6 different continental regions (hereafter, CR), shown in Fig. 6, representing the annual mean of cloud droplet number columns for ST-STN and ST-HYB (CDNC), which are again similar to the results of the RH simulations. Note that CDNC reflects the CCN column burden. The CCN and CDNC from RH-CLC can be found in the Supplement. Table 7 shows the summary of the dominant aerosol types and their compositions based on the global distribution of aerosol column burden in Fig. S1 in the Supplement, which resembles the aerosol distribution in the study of Pringle et al. (2010a), (see their Figs. 6 and 7 and their evaluation). Figure 7 presents the vertical profiles of aerosol activities (AF_i) in the selected continental regions (CRs) for ST-STN and ST-HYB. The estimated AF_i do not depend much on the choice of CLC scheme and therefore we present only results of the ST-simulations. To illustrate the regional variability depending on aerosol composition and meteorological conditions, the relevant cloud properties, i.e., cloud water, ice, and cloud cover are shown in Supplement Figs. S6, S8, and 8,

ACPD
14, 21975–22043, 2014

respectively. The estimated cloud radiative effects at TOA for all simulations and the observations are presented in Fig. 9.

For all selected continental regions, the total activated fraction of STN is L-shaped with high aerosol activation in the PBL (Fig. 7), in contrast to the funnel-shaped profile from HYB due to the lower aerosol activation fraction in the PBL. This impacts low (warm) cloud formation, with enhanced cloud cover especially for ST-CLC (Fig. 8) and enhanced cloud water for both CLC schemes (Supplement Fig. S6). Furthermore the ST-CLC scheme generally responds more sensitively to changes in the activated fraction.

Figure 6 shows that both simulations (ST-STN and ST-HYB) produce maxima in column cloud droplet number in CR1 as this region is highly polluted with high concentrations of sulfate, dust, nitrate and ammonium, the latter illustrated in Supplement Fig. S1. Note that the hygroscopicity of aerosols in the upper PBL and lower- most troposphere is depressed by a high loading of dust particles and thereby a low activated fraction (e.g., compared to region CR3) in ST-HYB.

From the surface to the PBL height ST-STN produces larger cloud fractions with a large amount of cloud water and higher CCN concentrations in all size modes compared to ST-HYB. It enhances optically thick cloud cover near the surface and predicts a strong cloud albedo effect. For mid level (above 4 km) and high clouds the response to aerosol–cloud interaction is more subtle. Despite the fact that ST-STN simulates a higher number of CCN (Figs. 7 and Supplement Fig. S3), ST-HYB produces a more extensive high cloud cover. This is associated with larger amounts of cloud ice and ICNC (Figs. S7 and S5 in the Supplement), and by weakened convection in ST-STN due to surface cooling by enhanced low clouds, which is reflected in lower cloud top height and lower relative humidity than in ST-HYB (Supplement Fig. S8). These effects are also found for RH-STN and RH-HYB, but much weaker. The aerosol–cloud interactions in the RH-simulations influence predominantly the cloud water content up to 4 km, which is more than doubled in RH-STN compared to RH-HYB; the influence on cloud cover is minor. The large impact of aerosol activation on low (warm) cloud formation is

ACPD
14, 21975–22043, 2014

also clearly reflected in the radiative properties, which are dominated by changes in the short wave cloud radiative effect (SCRE, Fig. 9): we obtain differences of $-18\,W\,m^{-2}$ for RH-STN and RH-HYB, and of $-28\,W\,m^{-2}$ for ST-STN and ST-HYB. In accordance with increased high clouds, the long wave cloud radiative heating is increased in the HYB simulations, which are generally closer to observations especially for SCRE. Note that the uncertainty ranges of the observations in Fig. 9 are same as in Table 5 (CERES EBAF Edition2.6r Data Quality Summary).

Maxima of OC and BC occur over Central Africa and South America (CR2 and CR5), being biomass burning areas. The regions CR2 and CR5 show similarity in the vertical distribution of the activated aerosol fraction (AF), cloud cover, and cloud ice distribution, and cloud water distribution sensitively responds to the simulated cloud droplet number concentration. The aerosol composition leads to a relatively low aerosol activity in the regions CR2 and CR5 though with different magnitudes, particularly near the surface. Region CR2 has more particles with low hygroscopicity (BC, OC, DU) and less hygroscopic particles (e.g., sea spray) than region CR5. These differences significantly impact the cloud radiative effects (Fig. 9b and e) by changes in the cloud vertical structure and optical properties. The simulations for region CR5 show larger cloud fractions with larger cloud droplet number concentrations and condensed water than in region CR2. The changes in low clouds intensify the cloud albedo effect (SCRE) and lead to stronger cooling in CR5 than in CR2.

Aloft these particles can become more hygroscopic by chemical (ageing) processes with consequences for CCN and IN and the properties of high clouds. The clouds in both regions are simulated to have two maxima, in the PBL and near the tropopause, being particularly pronounced in the RH-simulations (see Fig. 8b and e). The predicted high clouds in the HYB-simulations are more extensive than in the STN-simulation and contribute to the greenhouse effects (LCRE), hence causing a stronger LCRE compared to the STN simulations. In the STN-simulations, for both CR2 and CR5 the SCRE is overestimated and LCRE is underestimated, and are therefore the net cooling effect is too strong. Overall, the estimates of CREs in ST-HYB are relatively close to the

ACPD
14, 21975–22043, 2014

observations. As in CR1, the enhanced low clouds weaken convective activity causing reduced high cloud formation in the STN-simulations.

Over Europe (CR3) significantly enhanced concentrations of sulfate (more than $5\,mg\,m^{-2}$), nitrate and ammonium (more than $2\,mg\,m^{-2}$) are found. The Aitken mode aerosols are relatively highly hygroscopic compared to the other regions. The aerosol composition in region CR6 over the sub Arctic and Siberia is not very different from CR3. This region has more dust, slightly more BC and OC, and more sea spray from the Mediterranean Sea and Atlantic Ocean (the western section) and therefore has slightly higher activity (AF) than region CR6.

The simulated cloud condensate in the regions CR3 and CR6 is concentrated in the lower troposphere with a significant fraction of ice, more than in the other regions due to colder temperatures at these latitudes. In CR6 the simulated low cloud cover (haze and fog) is twice as high compared to CR3 with more cloud ice and liquid water. These differences also affect the cloud radiative effects. So for both regions the changes in the net cloud radiative forcing are dominated by changes in SCRE, and ST-CLC is approximately twice as sensitive to supersaturation parameterization; CR3Δ(RH-STN – RH-HYB) = $-12\,W\,m^{-2}$, Δ(ST-STN – ST-HYB) = $-20\,W\,m^{-2}$. Especially in the short wave radiation regime the clouds over Arctic Siberia respond strongly to aerosol–cloud coupling (Δ(RH-STN – RH-HYB) = $-15\,W\,m^{-2}$, Δ(ST-STN – ST-HYB) = $-30\,W\,m^{-2}$). Comparing the CDN schemes we find that the STN-simulations usually overpredict the cooling effect (SCRE), while the HYB-simulation results agree reasonably well with the observations.

Over North Africa and the Arabian Peninsula (CR4) a major fraction of the aerosol is dust emitted from the deserts, and the annual mean aerosol column exceeds $200\,mg\,m^{-2}$; additionally sulfate concentrations are relatively high (Fig. S1 in the Supplement). The simulated cloud cover is highest at high altitudes but is relatively minor at all altitudes compared to other regions. These high clouds, i.e., thin cirrus, exert a positive NCRE (Chen et al., 2000). All simulations consistently predict stronger longwave than shortwave cloud effects. The calculated LCREs tend to be slightly larger

ACPD
14, 21975–22043, 2014

with RH-CLC than with ST-CLC due to the larger amount of cloud ice and high clouds in the RH-simulations. The cloud liquid water and cloud droplet numbers at low altitudes are generally increased by the large number concentration of activated CCN. In this region the changes in the net cloud radiative forcing are dominated by changes in LCRE. For CR4 the modeled CREs in all simulations are close to those observed by CERES. Overall, the simulated clouds and cloud radiative effects are found to be sensitive to aerosol–cloud feedbacks, and are influenced by particle composition, size and number concentration.

3.4 General assessment

This section summarizes the global performance of the CDN parameterizations in combination with the CLC schemes in the EMAC model. The multi-year means of model simulations and observational data are compared using a Taylor diagram (Taylor, 2001) to evaluate spatial pattern similarity with observations. Although the measurements have not been performed during the same time periods (Table 5) as the model simulations it may be assumed that these differences are minor. All comparisons are based on the re-gridded observational data to the horizontal resolution of the model (T42, about 2.8°). In order to plot different fields (parameters) on the same diagram, the statistic variables, i.e., the centered root mean square difference and the two standard deviation (of the model results and observations), are normalized by the standard deviations of the observations. Figure 10 demonstrates the (dis)similarity between the simulations and the observations (OBS) using the normalized centered root mean square difference (CRMS, gray arcs), ratio of modelled to observed variability (straight axes, dashed arcs) and the correlation coefficient on the curved axis (gray dashed radii), separately for land and ocean. Furthermore, the information in the Taylor diagram has been condensed into a skill score in Table 9 (using Eq. 4 of Taylor, 2001), which allows ranking of the simulations with respect to observations. Over land, we generally find a higher correlation than over the ocean (0.8–0.9 vs. 0.7–0.8) and also lower CRMS

ACPD
14, 21975–22043, 2014

errors and more realistic variability, with the remarkable exception of continental total precipitation of ST-REF and ST-HYB and of SCRE of RH-STN and ST-STN.

For the simulated total cloud cover the spatial pattern similarity is mostly determined by the cloud cover scheme, over continents and even more pronounced for marine clouds, as compared to the MODIS observations between 60° N and 60° S. As mentioned earlier the satellite retrievals are less reliable over bright surfaces (i.e., high albedo areas) such as deserts and glacial (snow or ice) regions, e.g., over Antarctica, the Arctic Ocean and polar regions. We typically find substantial positive biases over these regions (Supplement Fig. S10), which can be attributed to an underestimation of clouds in the satellite data rather than model error. The high latitude regions are therefore excluded from the comparison.

All the RH-simulations have the same high correlation of 0.9 and have the same standard deviation as the observations and low CRMS errors, with slightly better performance over land than over the ocean. The sensitivity of TCC to aerosol- cloud coupling is not distinct in the RH-simulations. On the other hand, the ST-CLC configurations are more sensitive to the aerosol–cloud coupling. The ST-REF simulation performs worse considering all three statistical parameters and is clearly improved with interactive aerosol. The higher dissimilarities in the total cloud cover in the ST-simulations are mainly caused by the underestimation of tropical and subtropical marine clouds, as discussed above and in Weber et al. (2011), see Fig. S10 in the Supplement.

The spatial pattern comparison to CERES observations for the cloud radiative effects confirms the previous finding that aerosol–cloud coupling mostly affects low clouds and the experimental set-up therefore has less impact on the LCRE than the SCRE, particularly over land. In general, the statistical parameters representing SCRE and LCRE indicate a larger scatter over land than over the ocean. Over land, the representation of SCRE groups into 3 categories related to the choice of the CLC and CDN schemes; two of them are distinct to the cloud cover scheme (RH-REF and RH-HYB; ST-REF and ST-HYB) and show very similar statistical performance, and the outlier group is governed by the CDN scheme (RH-STN and ST-STN). The LCRE reveals basically

ACPD
14, 21975–22043, 2014

the same pattern as the SCRE but within a smaller range. Over the ocean, the SCRE shows a weak grouping according to the aerosol–cloud coupling, and for LCRE the grouping is determined by the cloud cover scheme, where the RH-simulations are very close to each other.

The model calculated total precipitation (P_{tot}) in all simulations shows high pattern correlations (higher than 0.8) with the observations (GPCP). Over land, the plotted P_{tot} shows a much larger spread than over the ocean due to the prescribed SST and SIC. They are grouped into three by the cloud cover scheme (ST-REF and ST-HYB, and RH-REF and RH-HYB) and by the CDN scheme (RH-STN and ST-STN). ST-STN reproduces the observed P_{tot} remarkably well, whereas the other ST setups are clearly biased. Over the ocean, the statistical parameters of P_{tot} indicate less spread and are grouped according to the cloud cover scheme. The aerosol–cloud coupling is of minor influence. As discussed above, we expect that total precipitation is generally further improved by increasing the vertical and horizontal resolution (Hagemann et al., 2006; Roeckner et al., 2006).

Overall, the Taylor skill scores also indicate that the current EMAC model configuration performs better over land than over the ocean. The RH-simulations have a larger spread in the average skill score, with the exception of RH-STN which performs better than the ST configurations. Obviously for the RH-CLC setups the κ activation method (HYB) is the best choice, as can be seen from the average scores and from the individual skill scores for the meteorological parameters. Over land, also for ST-CLC, the HYB CDN scheme is a better choice even it is not so obvious in average skill score. The radiation feedback and total precipitation improve in ST-HYB compared to ST-REF, whereas in ST-STN poor performance in representing radiative effects contrasts with the strong improvement in P_{tot}. Over the ocean, a clear recommendation of the aerosol–cloud coupling for the ST-CLC is not obviously made based on the skill score.

ACPD
14, 21975–22043, 2014

4 Summary and conclusions

In this study we compared the STN (osmotic coefficient model) and HYB (κ hygroscopicity parameter) schemes to consider aerosol–cloud feedbacks with a focus on warm clouds. The simulations show substantial cloud radiative effects from CCN activation, especially in low clouds. In the STN simulations, large fractions of aerosols are activated as CCN in warm clouds and fogs/hazes near the surface. Anthropogenically enhanced CCN concentrations at low altitudes enhance the cloud albedo effect (SCRE), which cools the Earth's surface. The cooler surface leads to reduced convection and associated precipitation through the increased hydrostatic stability in the lower troposphere. At the same time, condensation into cloud droplets releases latent heat and invigorates convective activity. Over land, the first effect prevails and the simulations with aerosol–cloud coupling show reduced convective activity, more pronounced in the STN simulations (−23 to −35 % in CAPE) than in the HYB simulations (about −5 %), see Table 10. For the marine environment with prescribed SST the latter effect dominates which leads to increased convective activity. Note that for high CDNC the CAPE in statistical cloud cover setups responds substantially more strongly to the aerosol–cloud coupling than with the RH-CLC scheme.

The changes in low cloud properties induced by CCN abundance (and activated fraction) are therefore very important to climate. Furthermore, the effects of aerosol–cloud interactions vary strongly geographically as shown by the analysis of the selected six continental regions for which the sensitivities of cloud properties (cloud cover, CDNC, ICNC, LWC and IWC) to CCN (aerosol activation) have been shown. The comparison of ST-REF and the observations indicates a strongly underestimated SCRE and NCRE, indicative of deficiencies in representing the climate system in the reference setup of the model. It underscores that in climate simulations aerosol–cloud feedbacks are important and should be considered prognostically rather than using fixed parameters in cloud formation processes. This applies particularly to the cloud model coupled with a cloud cover scheme that is sensitive to aerosol–cloud feedbacks (e.g., ST-CLC). The

ACPD
14, 21975–22043, 2014

short wave cloud radiative effect at the top of the atmosphere in the ST-CLC simulations responds a factor of 2–8 more sensitively to aerosol coupling than in the RH-CLC setups. The long wave cloud radiative sensitivity among the different scheme varies within a factor of 2, (Fig. 10, which is based on the numbers of Table 8). The sensitivity is defined as the ratio of the relative differences.

The current study clearly shows the sensitivity of aerosol activation patterns and cloud properties in response to the representation of aerosol chemistry, hence hygroscopicity and critical supersaturation. Both prognostic CDN schemes (STN and HYB) account for the aerosol size and composition effects on droplet nucleation in warm clouds. The HYB CDN representation performs best with both cloud cover schemes, the coupling with STN leads to unrealistically high fractions of activated CCN. The simulated cloud properties and CREs are relatively close to observations, particularly over the continents (relatively high aerosol concentrations), as shown by reduced biases in TCC and NCRE, and realistic distributions of droplet number and LWP. ST-CLC generally shows much higher sensitivity to aerosol–cloud coupling, but deficiencies in simulating marine stratiform clouds remain.

Furthermore, the HYB scheme shows a higher sensitivity of CCN activation to chemical composition, which is particularly relevant for Aitken mode particles. In general, cloud properties and other parameters relevant to the hydrologic cycle and climate are more realistically represented by prognostic CDN and CLC schemes. Globally, Aitken mode particles are the primary source for CDNC, independently of the choice of CDN and CLC scheme. Although in polluted regions the abundance of accumulation and coarse mode aerosols can suppress the activation of large numbers of Aitken mode particles, on a global scale the latter are important with a significant activated fraction of CCN (the majority in all schemes). Since for small particles the chemical composition, i.e., the solute (Raoult) effect, is more critical than for larger aerosols, we find a relatively strong overall sensitivity of CCN activation to chemical composition. Our results corroborate that aerosol chemistry matters because the aerosol size matters,

ACPD
14, 21975–22043, 2014

and indirect climate effects through clouds are governed by anthropogenic changes in aerosol number concentration and composition.

The Supplement related to this article is available online at doi:10.5194/acpd-14-21975-2014-supplement.

Acknowledgements. We thank U. Lohmann for providing the cloud microphysics scheme. We further thank all EMAC developers and modelers for providing code and support. We also thank the DKRZ for providing high-performance computing support. Additionally, we would like to acknowledge use of FERRET for analysis and graphics in this work. Ferret is a product of NOAA's Pacific Marine Environmental Laboratory (information is available online at http://ferret.pmel.noaa.gov/Ferret/). The research leading to these results has received funding from the European Research Council under the European Union's Seventh Framework Programme (FP7/2007-2013)/ERC grant agreement no. 226144.

The service charges for this open access publication have been covered by the Max Planck Society.

References

Abdul-Razzak, H. and Ghan, S. J.: A parameterization of aerosol activation 2. Multiple aerosol types, J. Geophys. Res., 105, 6837–6844, 2000.

Abdul-Razzak, H. and Ghan, S. J.: A parameterization of aerosol activation: 3. Sectional representation, J. Geophys. Res., 107, 4026, doi:10.1029/2001JD000483, 2002.

Abdul-Razzak, H. and Ghan, S. J.: Parameterization of the influence of organic surfactants on aerosol activation, J. Geophys. Res., 109, D03205, doi:10.1029/2003JD004043, 2004.

Abdul-Razzak, H., Ghan, S. J., and Rivera-Carpio, C.: A parameterization of aerosol activation: 1. Single aerosol type, J. Geophys. Res.,103, 6123–6132, 1998.

Adler, R. F., Huffman, G. J., Chang, A., Ferraro, R., Xie, P., Janowiak, J., Rudolf, B., Schneider, U., Curtis, S., Bolvin, D., Gruber, A., Susskind, J., Arkin, P., and Nelkin, E.: The version-

ACPD
14, 21975–22043, 2014

2 global precipitation climatology project (GPCP) monthly precipitation analysis (1979–present), J. Hydrometeorol., 4, 1147–1167, 2003.
Ackerman, A. S., Toon, O. B., Stevens, D. E., Heymsfield, A. J., Ramanathan, V., and Welton, E. J.: Reduction of tropical cloudiness by soot, Science, 288, 1042–1047, 2000.
Albrecht, B.: Aerosols, cloud microphysics, and fractional cloudiness, Science, 245, 1227–1230, 1989.
Anderson, T. L., Charlson, R. J., Schwartz, S. E., Knutti, R., Boucher, O., Rodhe, H., and Heintzenberg, J.: Climate forcing by aerosols – a hazy picture, Science, 300, 1103–1104, 2003.
Andreae, M. O. and Rosenfeld, D.: Aerosol–cloud-precipitation interactions, Part 1: The nature and sources of cloud-active aerosols, Earth Sci. Rev., 89, 13–41, doi:10.1016/j.earscirev.2008.03.001, 2008.
Boucher, O. and Lohmann, U.: The sulfate-CCN-cloud albedo effect: a sensitivity study with two general circulation models, Tellus B, 47, 281–300, 1995.
Bougiatioti, A., Fountoukis, C., Kalivitis, N., Pandis, S. N., Nenes, A., and Mihalopoulos, N.: Cloud condensation nuclei measurements in the marine boundary layer of the Eastern Mediterranean: CCN closure and droplet growth kinetics, Atmos. Chem. Phys., 9, 7053–7066, doi:10.5194/acp-9-7053-2009, 2009.
Cess, R. D., Potter, G. L., Blanchet, J. P., Boer, G. J., Del Genio, A. D., Deque, M., Dymnikov, V., Galin, V., Gates, W. L., Ghan, S. J., Kiehl, J. T., Lacis, A. A., Le Treut, H., Li, Z.-X., Liang, X.-Z., McAvaney, B. J., Meleshko, V. P., Mitchell, J. F. B., Morcrette, J.-J., Randall, D. A., Rikus, L., Roeckner, E., Royer, J. F., Schlese, U., Sheinin, D. A., Slingo, A., Sokolov, A. P., Taylor, K. E., Washington, W. M., Wetherald, R. T., Yagai, I., and Zhang, M.-H.: Intercomparison and interpretation of climate feedback processes in 19 atmospheric general circulation models, J. Geophys. Res., 95, 16601–16615, 1990.
Cess, R. D., Zhang, M. H., Ingram, W. J., Potter, G. L., Alekseev, V., Barker, H. W., Cohen-Solal, E., Colman, R. A., Dazlich, D. A., Del Genio, A. D., Dix., M. R., Dymnikov, V., Esch, M., Fowler, L. D., Fraser, J. R., Galin, V., Gates, W. L., Hack, J. J., Kiehl, J. T., Le Treut, K.-W. K., McAvaney, B. J., Meleshko, V. P., Morcrette, J.-J., Randall, D. A., Roeckner, E., Royer, J.-F., Schlesinger, M. F., Sporyshev, P. V., Timbal, B., Volodin, E. M., Taylor, K. E., and Wetherald, R. T.: Cloud feedback in atmospheric general circulation models: an update, J. Geophys. Res., 101, 12791–12794, 1996.

ACPD
14, 21975–22043, 2014

Chen, T., Rossow, W. B., and Zhang, Y.: Radiative effects of cloud-type variations, J. Climate, 13, 264–286, 2000.
Chu, D., Kaufman, Y., Ichoku, C., Remer, L., Tanre, D., and Holben, B.: Validation of MODIS aerosol optical depth retrieval over land, Geophys. Res. Lett., 29, 8007, doi:10.1175/JAS3385.1, 2002.
Chuang, C. C. and Penner, J. E.: Effects of anthropogenic sulfate on cloud drop nucleation and optical properties, Tellus B, 47, 566–577, 1995.
Cohard, J. M., Pinty, J. P., and Suhre, K.: On the parameterization of activation spectra from cloud condensation nuclei microphysical properties, J. Geophys. Res., 105, 11753–11766, doi:10.1029/1999JD901195, 2000.
de Meij, A., Pozzer, A., Pringle, K. J., Tost, H., and Lelieveld, J.: EMAC model evaluation and analysis of atmospheric aerosol properties and distribution, Atmos. Res., 114–115, 38–69, 2012.
Dentener, F., Kinne, S., Bond, T., Boucher, O., Cofala, J., Generoso, S., Ginoux, P., Gong, S., Hoelzemann, J. J., Ito, A., Marelli, L., Penner, J. E., Putaud, J.-P., Textor, C., Schulz, M., van der Werf, G. R., and Wilson, J.: Emissions of primary aerosol and precursor gases in the years 2000 and 1750 prescribed data-sets for AeroCom, Atmos. Chem. Phys., 6, 4321–4344, doi:10.5194/acp-6-4321-2006, 2006.
Devasthale, A., Kruger, O., and Grassl, H.: Change in cloud-top temperatures over Europe, IEEE Geosci. Remote S., 2, 333–336, doi:10.1109/LGRS.2005.851736, 2005.
Dusek, U., Frank, G. P., and Hildebrandt, L.: Size matters more than chemistry for cloud-nucleating ability of aerosol particles, Science, 312, 1375–1378, 2006.
Dusek, U., Frank, G. P., Curtius, J., Drewnick, F., Schneider, J., Küurten, A., Rose, D., Andreae, M. O., Borrmann, S., and Pöschl, U.: Enhanced organic mass fraction and decreased hygroscopicity of cloud condensation nuclei (CCN) during new particle formation events, Geophys. Res. Lett., 37, L03804, doi:10.1029/2009GL040930, 2010.
Feichter, J., Lohmann, U., and Schult, I.: The atmospheric sulfur cycle and its impact on the shortwave radiation, Clim. Dynam., 13, 235–246, 1997.
Feingold, G.: Modeling of the first sindirect effect: analysis of measurement requirements, Geophys. Res. Lett., 30, 1997, doi:10.1029/2003GL017967, 2003.
Feingold, G. and Heymsfield, A.: Parameterizations of condensational growth of droplets for use in general circulation models, J. Atmos. Sci., 49, 2325–2342, 1992.

ACPD
14, 21975–22043, 2014

Feingold, G., Eberhard, W. L., Veron, D. E., and Previdi, M.: First measurements of the Twomey indirect effect using ground-based remote sensors, Geophys. Res. Lett., 30, 1287, doi:10.1029/2002GL016633, 2003.
Forster, P., Ramaswamy, V., Artaxo, P., Berntsen, T., Betts, R., Fahey, D., Haywood, J., Lean, J., Lowe, D., Myhre, G., Nganga, J., Prinn, R., Raga, G. M. S., and Dorland, R. V.: Changes in atmospheric constituents and in radiative forcing, in: Intergovernmental Panel on Climate Change, Cambridge University Press, Cambridge, UK, New York, NY, USA, 130–234, 2007.
Fountoukis, C. and Nenes, A.: Continued development of a cloud droplet formation parameterization for global climate models, J. Geophys. Res., 110, D11212, doi:10.1029/2004JD005591, 2003.
Gerald, G. M., Houser, S., Benson, S., Stephen, A., Klein, S. A., and Min, Q.: Critical evaluation of the ISCCP simulator using ground-based remote sensing data, J. Climate, 24, 1598–1612, doi:10.1175/2010JCLI3517.1, 2011
Ghan, S., Chuang, C., and Penner, J.: A parameterization of cloud droplet nucleation, Part I: Single aerosol species, Atmos. Res., 30, 197–222, 1993.
Ghan, S., Chuang, C., Easter, R., and Penner, J.: A parameterization of cloud droplet nucleation: 2. Multiple aerosol types, Atmos. Res., 36, 39–54, 1995.
Ghan, S. J., Leung, L. R., Easter, R. C., and Abdul-Razzak, H.: Prediction of cloud droplet number in a general circulation model, J. Geophys. Res., 102, 21777–21794, 1997.
Gultepe, I. and Isaac, G. A.: The relationship between cloud droplet and aerosol number concentrations for climate models, Int. J. Climatol., 16, 1–6, 1996.
Gunthe, S. S., King, S. M., Rose, D., Chen, Q., Roldin, P., Farmer, D. K., Jimenez, J. L., Artaxo, P., Andreae, M. O., Martin, S. T., and Pöschl, U.: Cloud condensation nuclei in pristine tropical rainforest air of Amazonia: size-resolved measurements and modeling of atmospheric aerosol composition and CCN activity, Atmos. Chem. Phys., 9, 7551–7575, doi:10.5194/acp-9-7551-2009, 2009.
Hagemann, S., Arpe, K., and Roeckner, E.: Evaluation of the Hydrological Cycle in the ECHAM5 Model. J. Climate, 19, 3810–3827, doi:10.1175/JCLI3831.1, 2006.
Han, Q., Rossow, W. B., and Lacis, A. A.: Near-global survey of effective droplet radii in liquid water clouds using ISCCP data, J. Climate, 7, 465–497, 1994.
Han, Q., Rossow, W. B., Chou, J., and Welch, R. M.: Global survey of the relationships of cloud albedo and liquid water path with droplet size using ISCCP, J. Climate, 11, 1516–1528, 1998.

ACPD
14, 21975–22043, 2014

Hänel, G.: The role of aerosol properties during the condensational stage of cloud: a reinvestigation of numerics and microphysics, Beitr. Phys. Atmos., 60, 321–339, 1987.
Haywood, J. and Schulz, M.: Causes for the reduction of uncertainty in estimates of the anthropogenic radiative forcing of climate between IPCC (2001) and IPCC (2007), Geophys. Res. Lett., 34, L20701, doi:10.1029/2007GL030749, 2007.
Henning, S., Wex, H., Hennig, T., Kiselev, A., Snider, J., Rose, D., Dusek, U., Frank, G. P., Pöschl, U., Kristensson, A., Bilde, M., Tillmann, R., Kiendler-Scharr, A., Mentel, T. F., Walter, S., Schneider, J., Wennrich, C., and Stratmann, F.: Soluble mass, hygroscopic growth and droplet activation during LExNo, J. Geophys. Res., 115, D11206, doi:10.1029/2009JD012626, 2010.
Hoose, C., Lohmann, U., Stier, P., Verheggen, B., and Weingartner, E.: Aerosol processing in mixed-phase clouds in ECHAM5-HAM: model description and comparison to observations, J. Geophys. Res., 113, D07210, doi:10.1029/2007JD009251, 2008
IAPSAG: WMO/IUGG International Aerosol Precipitation Science Assessment Group (IAPSAG) Report: Aerosol Pollution Impact on Precipitation: a Scientific Review, World Meteorological Organization, Geneva, 482 pp., 2007.
IPCC core writing team: IPCC, 2007: Climate Change 2007: Synthesis Report, Contribution of Working Groups I, II and III to the Fourth Assessment Report of the Intergovernmental Panel on Climate Change, IPCC, Geneva, Switzerland, 2007.
IPCC core writing team: IPCC, 2013: Climate Change 2013: Synthesis Report, Contribution of Working Groups I, II and III to the Fifth Assessment Report of the Intergovernmental Panel on Climate Change, IPCC, Geneva, Switzerland, 2013.
Jiang, J. H., Su, H., Zhai, C., Perun, V., Del Genio, A. D., Nazarenko, L. S., Donner, L. J., Horowitz, L. W., Seman, C. J., Cole, J., Gettelman, A., Ringer, M. A., Rotstayn, L. D., Jeffrey, S. J., Wu, T., Brient, F., Dufresne, J.-L., Kawai, H., Koshiro, T., Masahiro, W., LÉcuyer, T. S., Volodin, E. M., Iversen, T., Drange, H., dos Santos Mesquita, M., Read, W. G., Waters, J. W., Tian, B., Teixeira, J., and Stephens, G. L.: Evaluation of cloud and water vapor simulations in CMIP5 climate models using NASA “A-Train” satellite observations, J. Geophys. Res., 117, D14105, doi:10.1029/2011JD017237, 2012.
Jones, A. and Slingo, A.: Predicting cloud-droplet effective radius and indirect sulphate aerosol forcing using a general circulation model, Q. J. Roy. Meteor. Soc., 122, 1573–1595, 1996.
Jones, A., Roberts, D. L., and Slingo, A.: A climate model study of indirect radiative forcing by anthropogenic sulphate aerosols, Nature, 370, 450–453, 1994.

ACPD
14, 21975–22043, 2014

Jöckel, P., Sander, R., Kerkweg, A., Tost, H., and Lelieveld, J.: Technical Note: The Modular Earth Submodel System (MESSy) – a new approach towards Earth System Modeling, Atmos. Chem. Phys., 5, 433–444, doi:10.5194/acp-5-433-2005, 2005.

Jöckel, P., Tost, H., Pozzer, A., Brühl, C., Buchholz, J., Ganzeveld, L., Hoor, P., Kerkweg, A., Lawrence, M. G., Sander, R., Steil, B., Stiller, G., Tanarhte, M., Taraborrelli, D., van Aardenne, J., and Lelieveld, J.: The atmospheric chemistry general circulation model ECHAM5/MESSy1: consistent simulation of ozone from the surface to the mesosphere, Atmos. Chem. Phys., 6, 5067–5104, doi:10.5194/acp-6-5067-2006, 2006.

Jöckel, P., Kerkweg, A., Buchholz-Dietsch, J., Tost, H., Sander, R., and Pozzer, A.: Technical Note: Coupling of chemical processes with the Modular Earth Submodel System (MESSy) submodel TRACER, Atmos. Chem. Phys., 8, 1677–1687, doi:10.5194/acp-8-1677-2008, 2008.

Kärcher, B. and Lohmann, U.: A parameterization of cirrus cloud formation: homogeneous freezing including effects of aerosol size, J. Geophys. Res., 107, 4698, doi:10.1029/2001JD001429, 2002

Kaufman, Y. J. and Fraser, R. S.: The effect of smoke particles on clouds and climate forcing, Science, 277, 1636–1639, 1997.

Kaufman, Y., Tanre, D., Remer, L., Vermote, E., Chu, A., and Holben, B.: Operational remote sensing of tropospheric aerosol over land from EOS moderate resolution imaging spectroradiometer, J. Geophys. Res., 102, 17051–17067, doi:10.1029/96JD03988, 1997.

Kazil, J., Stier, P., Zhang, K., Quaas, J., Kinne, S., O'Donnell, D., Rast, S., Esch, M., Ferrachat, S., Lohmann, U., and Feichter, J.: Aerosol nucleation and its role for clouds and Earth's radiative forcing in the aerosol-climate model ECHAM5-HAM, Atmos. Chem. Phys., 10, 10733–10752, doi:10.5194/acp-10-10733-2010, 2010.

Kerkweg, A., Buchholz, J., Ganzeveld, L., Pozzer, A., Tost, H., and Jöckel, P.: Technical Note: An implementation of the dry removal processes DRY DEPosition and SEDImentation in the Modular Earth Submodel System (MESSy), Atmos. Chem. Phys., 6, 4617–4632, doi:10.5194/acp-6-4617-2006, 2006a.

Kerkweg, A., Sander, R., Tost, H., and Jöckel, P.: Technical note: Implementation of prescribed (OFFLEM), calculated (ONLEM), and pseudo-emissions (TNUDGE) of chemical species in the Modular Earth Submodel System (MESSy), Atmos. Chem. Phys., 6, 3603–3609, doi:10.5194/acp-6-3603-2006, 2006b.

ACPD
14, 21975–22043, 2014

Khairoutdinov, M. and Kogan, Y.: A new cloud physics parameterization in a large-eddy simulation model of marine stratocumulus, Mon. Weather Rev., 128, 229–243, 2000.
Khvorostyanov, V. I. and Curry, J. A.: Parameterization of cloud drop activation based on analytical asymptotic solutions to the supersaturation equation, J. Atmos. Sci., 66, 1905–1925, doi:10.1175/2009JAS2811.1, 2009.
Kim, D., Wang, C., Ekman, A. M. L., Barth, M. C., and Rasch, P. J.: Distribution and direct radiative forcing of carbonaceous and sulfate aerosols in an interactive size resolving aerosol climate model, J. Geophys. Res.-Atmos., 113, D16309, doi:10.1029/2007JD009756, 2008.
Kinne, S., Schulz, M., Textor, C., Guibert, S., Balkanski, Y., Bauer, S. E., Berntsen, T., Berglen, T. F., Boucher, O., Chin, M., Collins, W., Dentener, F., Diehl, T., Easter, R., Feichter, J., Fillmore, D., Ghan, S., Ginoux, P., Gong, S., Grini, A., Hendricks, J., Herzog, M., Horowitz, L., Isaksen, I., Iversen, T., Kirkevåg, A., Kloster, S., Koch, D., Kristjansson, J. E., Krol, M., Lauer, A., Lamarque, J. F., Lesins, G., Liu, X., Lohmann, U., Montanaro, V., Myhre, G., Penner, J., Pitari, G., Reddy, S., Seland, O., Stier, P., Takemura, T., and Tie, X.: An AeroCom initial assessment – optical properties in aerosol component modules of global models, Atmos. Chem. Phys., 6, 1815–1834, doi:10.5194/acp-6-1815-2006, 2006.
Koehler, K. A., Kreidenweis, S. M., DeMott, P. J., Petters, M. D., Prenni, A. J., and Carrico, C. M.: Hygroscopicity and cloud droplet activation of mineral dust aerosol, Geophys. Res. Lett., 36, L08805, doi:10.1029/2009GL037348, 2009.
Koren, I., Martins, J. V., Remer, L. A., and Afargan, H.: Smoke invigoration vs. inhibition of clouds over the Amazon, Science, 321, 946–949, 2008.
Kreidenweis, S. M., Petters, M. D., and Chuang, P. Y.: Cloud particle precursors, in: Clouds in the Perturbed Climate System: Their Relationship to Energy Balance, Atmospheric Dynamics, and Precipitation, Strüngmann Forum Report, edited by: Heintzenberg, J. and Charlson, R. J., The MIT Press, 13, Cambridge, Massachusetts, ISBN 978-0-262-01287-4, 291–317, 2009.
Lance, S., Nenes, A., and Rissman, T. A.: Chemical and dynamical effects on cloud droplet number: implications for estimates of the aerosol indirect effect, J. Geophys. Res., 109, D22208, doi:10.1029/2004JD004596, 2004.
Lauer, A., Eyring, V., Hendricks, J., Jöckel, P., and Lohmann, U.: Global model simulations of the impact of ocean-going ships on aerosols, clouds, and the radiation budget, Atmos. Chem. Phys., 7, 5061–5079, doi:10.5194/acp-7-5061-2007, 2007.

ACPD
14, 21975–22043, 2014

Levy, R. C., Remer, L. A., Kleidman, R. G., Mattoo, S., Ichoku, C., Kahn, R., and Eck, T. F.: Global evaluation of the Collection 5 MODIS dark-target aerosol products over land, Atmos. Chem. Phys., 10, 10399–10420, doi:10.5194/acp-10-10399-2010, 2010.
Loeb, N. G., Wielicki, B. A., Doelling, D. R., Smith, G. L., Keyes, D. F., Kato, S., Manalo-Smith, N., and Wong, N.: Toward optimal closure of the Earth's top-of-atmosphere radiation budget, J. Climate, 22, 748–766, 2009.
Lohmann, U. and Feichter, J.: Impact of sulfate aerosols on albedo and lifetime of clouds: a sensitivity study with the ECHAM4 GCM, J. Geophys. Res., 102, 13685–13700, 1997.
Lohmann, U. and Feichter, J.: Global indirect aerosol effects: a review, Atmos. Chem. Phys., 5, 715–737, doi:10.5194/acp-5-715-2005, 2005.
Lohmann, U. and Lesins, G.: Comparing continental and oceanic cloud susceptibilities to aerosols, Geophys. Res. Lett., 30, 1791, doi:10.1029/2003GL017828, 2003.
Lohmann, U., Feichter, J., Chuang, C. C., and Penner, J. E.: Prediction of the number of cloud droplets in the ECHAM GCM, J. Geophys. Res., 104, 9169–9198, 1999.
Lohmann, U., Stier, P., Hoose, C., Ferrachat, S., Kloster, S., Roeckner, E., and Zhang, J.: Cloud microphysics and aerosol indirect effects in the global climate model ECHAM5-HAM, Atmos. Chem. Phys., 7, 3425–3446, doi:10.5194/acp-7-3425-2007, 2007.
Lohmann, U., Rotstayn, L., Storelvmo, T., Jones, A., Menon, S., Quaas, J., Ekman, A. M. L., Koch, D., and Ruedy, R.: Total aerosol effect: radiative forcing or radiative flux perturbation?, Atmos. Chem. Phys., 10, 3235–3246, doi:10.5194/acp-10-3235-2010, 2010.
Mann, G. W., Carslaw, K. S., Reddington, C. L., Pringle, K. J., Schulz, M., Asmi, A., Spracklen, D. V., Ridley, D. A., Woodhouse, M. T., Lee, L. A., Zhang, K., Ghan, S. J., Easter, R. C., Liu, X., Stier, P., Lee, Y. H., Adams, P. J., Tost, H., Lelieveld, J., Bauer, S. E., Tsigaridis, K., van Noije, T. P. C., Strunk, A., Vignati, E., Bellouin, N., Dalvi, M., Johnson, C. E., Bergman, T., Kokkola, H., von Salzen, K., Yu, F., Luo, G., Petzold, A., Heintzenberg, J., Clarke, A., Ogren, J. A., Gras, J., Baltensperger, U., Kaminski, U., Jennings, S. G., O'Dowd, C. D., Harrison, R. M., Beddows, D. C. S., Kulmala, M., Viisanen, Y., Ulevicius, V., Mihalopoulos, N., Zdimal, V., Fiebig, M., Hansson, H.-C., Swietlicki, E., and Henzing, J. S.: Intercomparison and evaluation of global aerosol microphysical properties among AeroCom models of a range of complexity, Atmos. Chem. Phys., 14, 4679–4713, doi:10.5194/acp-14-4679-2014, 2014.
McFiggans, G., Artaxo, P., Baltensperger, U., Coe, H., Facchini, M. C., Feingold, G., Fuzzi, S., Gysel, M., Laaksonen, A., Lohmann, U., Mentel, T. F., Murphy, D. M., O'Dowd, C. D.,

ACPD
14, 21975–22043, 2014

Snider, J. R., and Weingartner, E.: The effect of physical and chemical aerosol properties on warm cloud droplet activation, Atmos. Chem. Phys., 6, 2593–2649, doi:10.5194/acp-6-2593-2006, 2006.
Menon, S., Del Genio, A. D., Koch, D., and Tselioudis, G.: GCM simulations of the aerosol indirect effect: sensitivity to cloud parameterization and aerosol burden, J. Atmos. Sci., 59, 692–713, 2002.
Mikhailov, E., Vlasenko, S., Martin, S. T., Koop, T., and Pöschl, U.: Amorphous and crystalline aerosol particles interacting with water vapor: conceptual framework and experimental evidence for restructuring, phase transitions and kinetic limitations, Atmos. Chem. Phys., 9, 9491–9522, doi:10.5194/acp-9-9491-2009, 2009.
Ming, Y., Ramaswamy, V., Donner, L. J., and Phillips, V. T. J.: A new parameterization of cloud droplet activation applicable to general circulation models, J. Atmos. Sci., 63, 1348–1356, doi:10.1175/JAS3686.1, 2006.
Moore, R. H., Cerully, K., Bahreini, R., Brock, C. A., Middlebrook, A. M., and Nenes, A.: Hygroscopicity and composition of California CCN during summer 2010, J. Geophys. Res., 117, D00V12, doi:10.1029/2011JD017352, 2012.
Nenes, A. and Seinfeld, J. H.: Parameterization of cloud droplet formation in global climate models, J. Geophys. Res., 108, 4415, doi:10.1029/2002JD002911, 2003.
Niedermeier, D., Wex, H., Voigtländer, J., Stratmann, F., Brüggemann, E., Kiselev, A., Henk, H., and Heintzenberg, J.: LACIS-measurements and parameterization of sea-salt particle hygroscopic growth and activation, Atmos. Chem. Phys., 8, 579–590, doi:10.5194/acp-8-579-2008, 2008.
Patra, P. K., Behera, S. K., Herman, J. R., Maksyutov, S., Akimoto, H., and Yamagata, Y.: The Indian summer monsoon rainfall: interplay of coupled dynamics, radiation and cloud microphysics, Atmos. Chem. Phys., 5, 2181–2188, doi:10.5194/acp-5-2181-2005, 2005.
Peng, Y. and Lohmann, U.: Sensitivity study of the spectral dispersion of the cloud droplet size distribution on the indirect aerosol effect, Geophys. Res. Lett., 30, 1507, doi:10.1029/2003GL017192, 2003.
Penner, J. E., Zhang, S. Y., and Chuang, C. C.: Soot and smoke aerosol may not warm climate, J. Geophys. Res., 108, 4657, doi:10.1029/2003JD003409, 2003.
Penner, J. E., Dong, X., and Chen, Y.: Observational evidence of a change in radiative forcing due to the indirect aerosol effect, Nature, 427, 231–234, 2004.

ACPD
14, 21975–22043, 2014

Penner, J. E., Quaas, J., Storelvmo, T., Takemura, T., Boucher, O., Guo, H., Kirkevåg, A., Kristjánsson, J. E., and Seland, Ø.: Model intercomparison of indirect aerosol effects, Atmos. Chem. Phys., 6, 3391–3405, doi:10.5194/acp-6-3391-2006, 2006.

Petters, M. D. and Kreidenweis, S. M.: A single parameter representation of hygroscopic growth and cloud condensation nucleus activity, Atmos. Chem. Phys., 7, 1961–1971, doi:10.5194/acp-7-1961-2007, 2007.

Pincus, R., Batstone, C. P., Hofmann, R. J. P., Taylor, K. E., and Gleckler, P. J.: Evaluating the present-day simulation of clouds, precipitation, and radiation in climate models, J. Geophys. Res., 113, D14209, doi:10.1029/2007JD009334, 2008.

Pöschl, U., Rose, D., and Andreae, M. O.: Climatologies of cloudrelated aerosols – Part 2: Particle hygroscopicity and cloud condensation nuclei activity, in: Clouds in the Perturbed Climate System, edited by: Heintzenberg, J. and Charlson, R. J., MIT Press, Cambridge, ISBN 978-0-262-012874, 58–72, 2009.

Posselt, R. and Lohmann, U.: Introduction of prognostic rain in ECHAM5: design and single column model simulations, Atmos. Chem. Phys., 8, 2949–2963, doi:10.5194/acp-8-2949-2008, 2008.

Pozzer, A., Pollmann, J., Taraborrelli, D., Jöckel, P., Helmig, D., Tans, P., Hueber, J., and Lelieveld, J.: Observed and simulated global distribution and budget of atmospheric C_2–C_5 alkanes, Atmos. Chem. Phys., 10, 4403–4422, doi:10.5194/acp-10-4403-2010, 2010.

Pozzer, A., de Meij, A., Pringle, K. J., Tost, H., Doering, U. M., van Aardenne, J., and Lelieveld, J.: Distributions and regional budgets of aerosols and their precursors simulated with the EMAC chemistry-climate model, Atmos. Chem. Phys., 12, 961–987, doi:10.5194/acp-12-961-2012, 2012.

Pringle, K. J., Tost, H., Message, S., Steil, B., Giannadaki, D., Nenes, A., Fountoukis, C., Stier, P., Vignati, E., and Lelieveld, J.: Description and evaluation of GMXe: a new aerosol submodel for global simulations (v1), Geosci. Model Dev., 3, 391–412, doi:10.5194/gmd-3-391-2010, 2010a.

Pringle, K. J., Tost, H., Pozzer, A., Pöschl, U., and Lelieveld, J.: Global distribution of the effective aerosol hygroscopicity parameter for CCN activation, Atmos. Chem. Phys., 10, 5241–5255, doi:10.5194/acp-10-5241-2010, 2010b.

Pruppacher, H. R. and Klett, J. D.: Microphysics of Clouds and Precipitation, Kluwer Acad. Publ., Dordrecht, 2000.

ACPD
14, 21975–22043, 2014

Quaas, J., Boucher, O., and Breon, F.-M.: Aerosol indirect effects in POLDER satellite data and the Laboratoire de Meteorologie Dynamique-Zoom (LMDZ) general circulation model, J. Geophys. Res., 109, D08205, doi:10.1029/2003JD004317, 2004.

Quaas, J., Boucher, O., Bellouin, N., and Kinne, S.: Satellite-based estimate of the direct and indirect aerosol climate forcing, J. Geophys. Res., 113, D05204, doi:10.1029/2007JD008962, 2008.

Quaas, J., Ming, Y., Menon, S., Takemura, T., Wang, M., Penner, J. E., Gettelman, A., Lohmann, U., Bellouin, N., Boucher, O., Sayer, A. M., Thomas, G. E., McComiskey, A., Feingold, G., Hoose, C., Kristjánsson, J. E., Liu, X., Balkanski, Y., Donner, L. J., Ginoux, P. A., Stier, P., Grandey, B., Feichter, J., Sednev, I., Bauer, S. E., Koch, D., Grainger, R. G., Kirkevåg, A., Iversen, T., Seland, Ø., Easter, R., Ghan, S. J., Rasch, P. J., Morrison, H., Lamarque, J.-F., Iacono, M. J., Kinne, S., and Schulz, M.: Aerosol indirect effects – general circulation model intercomparison and evaluation with satellite data, Atmos. Chem. Phys., 9, 8697–8717, doi:10.5194/acp-9-8697-2009, 2009.

Reichler, T. and Kim, J.: How well do coupled models simulate today's climate?, B. Am. Meteorol. Soc., 89, 303–311, doi:10.1175/BAMS-89-3-303, 2008

Reid, J. S., Eck, T. F., Christopher, S. A., Hobbs, P. V., and Holben, B. N.: Use of the Ångström exponent to estimate the variability of optical and physical properties of aging smoke particles in Brazil, J. Geophys. Res., 104, 27473–27489, 1999.

Reutter, P., Su, H., Trentmann, J., Simmel, M., Rose, D., Gunthe, S. S., Wernli, H., Andreae, M. O., and Pöschl, U.: Aerosol- and updraft-limited regimes of cloud droplet formation: influence of particle number, size and hygroscopicity on the activation of cloud condensation nuclei (CCN), Atmos. Chem. Phys., 9, 7067–7080, doi:10.5194/acp-9-7067-2009, 2009.

Roeckner, E., Brokopf, R., Esch, M., Giogetta, M., Hagemann, S., Kornblueh, L., Manzini, E., Schleese, U., and Schulzweida, U.: Sensitivity of simulated climate to horizontal and vertical resolution in the ECHAM5 atmosphere model, J. Climate, 19, 3771–3791, 2006.

Rose, D., Gunthe, S. S., Mikhailov, E., Frank, G. P., Dusek, U., Andreae, M. O., and Pöschl, U.: Calibration and measurement uncertainties of a continuous-flow cloud condensation nuclei counter (DMT-CCNC): CCN activation of ammonium sulfate and sodium chloride aerosol particles in theory and experiment, Atmos. Chem. Phys., 8, 1153–1179, doi:10.5194/acp-8-1153-2008, 2008.

Rose, D., Nowak, A., Achtert, P., Wiedensohler, A., Hu, M., Shao, M., Zhang, Y., Andreae, M. O., and Pöschl, U.: Cloud condensation nuclei in polluted air and biomass burning smoke near

ACPD
14, 21975–22043, 2014

the mega-city Guangzhou, China – Part 1: Size-resolved measurements and implications for the modeling of aerosol particle hygroscopicity and CCN activity, Atmos. Chem. Phys., 10, 3365–3383, doi:10.5194/acp-10-3365-2010, 2010.

Rose, D., Gunthe, S. S., Su, H., Garland, R. M., Yang, H., Berghof, M., Cheng, Y. F., Wehner, B., Achtert, P., Nowak, A., Wiedensohler, A., Takegawa, N., Kondo, Y., Hu, M., Zhang, Y., Andreae, M. O., and Pöschl, U.: Cloud condensation nuclei in polluted air and biomass burning smoke near the mega-city Guangzhou, China – Part 2: Size-resolved aerosol chemical composition, diurnal cycles, and externally mixed weakly CCN-active soot particles, Atmos. Chem. Phys., 11, 2817–2836, doi:10.5194/acp-11-2817-2011, 2011.

Rosenfeld, D.: Suppression of rain and snow by urban and industrial air pollution, Science, 287, 1793–1796, 2000.

Rotstayn, L. D., Cai, W., Dix, M. R., Farquhar, G. D., Feng, Y., Ginoux, P., Herzog, M., Ito, A., Penner, J. E., Roderick, M. L., and Wang, M.: Have Australian rainfall and cloudiness increased due to the remote effects of Asian anthropogenic aerosols?, J. Geophys. Res., 112, D09202, doi:10.1029/2006JD007712, 2007.

Ruehl, C. R., Chuang, P. Y., and Nenes, A.: Distinct CCN activation kinetics above the marine boundary layer along the California coast, Geophys. Res. Lett., 36, L15814, doi:10.1029/2009GL038839, 2009.

Sander, R., Kerkweg, A., Jöckel, P., and Lelieveld, J.: Technical note: The new comprehensive atmospheric chemistry module MECCA, Atmos. Chem. Phys., 5, 445–450, doi:10.5194/acp-5-445-2005, 2005.

Schwartz, S. E., Harshvardhan, and Benkovitz, C. M.: Influence of anthropogenic aerosol on cloud optical depth and albedo shown by satellite measurements and chemical transport modeling, P. Natl. Acad. Sci. USA, 99, 1784–1789, 2002.

Seinfeld, J. H. and Pandis, S. N.: Atmospheric Chemistry and Physics: From Air Pollution to Climate Change, Wiley, New York, 1998.

Shinozuka, Y., Clarke, A. D., DeCarlo, P. F., Jimenez, J. L., Dunlea, E. J., Roberts, G. C., Tomlinson, J. M., Collins, D. R., Howell, S. G., Kapustin, V. N., McNaughton, C. S., and Zhou, J.: Aerosol optical properties relevant to regional remote sensing of CCN activity and links to their organic mass fraction: airborne observations over Central Mexico and the US West Coast during MILAGRO/INTEX-B, Atmos. Chem. Phys., 9, 6727–6742, doi:10.5194/acp-9-6727-2009, 2009.

ACPD
14, 21975–22043, 2014

Shipway, B. J. and Abel, S. J.: Analytical estimation of cloud droplet nucleation based on an underlying aerosol population, Atmos. Res., 96, 344–355, doi:10.1016/j.atmosres.2009.10.005, 2010

Small, J. D., Chuang, P. Y., Feingold, G., and Jiang, H.: Can aerosol decrease cloud lifetime?, Geophys. Res. Lett., 36, L16806, doi:10.1029/2009GL038888, 2009.

Snider, J. R. and Petters, M. D.: Optical particle counter measurement of marine aerosol hygroscopic growth, Atmos. Chem. Phys., 8, 1949–1962, doi:10.5194/acp-8-1949-2008, 2008.

Snider, J. R., Wex, H., Rose, D., Kristensson, A., Stratmann, F., Hennig, T., Henning, S., Kiselev, A., Bilde, M., Burkhart, M., Dusek, U., Frank, G. P., Kiendler-Scharr, A., Mentel, T. F., Petters, M. D., and Pöschl, U.: Intercomparison of CCN and hygroscopic fraction measurements from LExNo, J. Geophys. Res., 115, D11205, doi:10.1029/2009JD012618, 2010.

Spracklen, D. V., Carslaw, K. S., Kulmala, M., Kerminen, V. M., Sihto, S. L., Riipinen, I., Merikanto, J., Mann, G. W., Chipperfield, M. P., Wiedensohler, A., Birmili, W., and Lihavainen, H.: Contribution of particle formation to global cloud condensation nuclei concentrations, Geophys. Res. Lett., 35, L06808, doi:10.1029/2007GL033038, 2008.

Stevens, B. and Feingold, G.: Untangling aerosol effects on clouds and precipitation in a buffered system, Nature, 461, 607–613, 2009.

Stier, P., Feichter, J., Kinne, S., Kloster, S., Vignati, E., Wilson, J., Ganzeveld, L., Tegen, I., Werner, M., Balkanski, Y., Schulz, M., Boucher, O., Minikin, A., and Petzold, A.: The aerosol-climate model ECHAM5-HAM, Atmos. Chem. Phys., 5, 1125–1156, doi:10.5194/acp-5-1125-2005, 2005.

Storelvmo, T., Kristjánsson, J.-E., and Lohmann, U.: Aerosol influence on mixed-phase clouds in CAM-Oslo, J. Atmos. Sci., 65, 3214–3230, 2008.

Su, H., Rose, D., Cheng, Y. F., Gunthe, S. S., Massling, A., Stock, M., Wiedensohler, A., Andreae, M. O., and Pöschl, U.: Hygroscopicity distribution concept for measurement data analysis and modeling of aerosol particle mixing state with regard to hygroscopic growth and CCN activation, Atmos. Chem. Phys., 10, 7489–7503, doi:10.5194/acp-10-7489-2010, 2010.

Sundqvist, H., Berge, E., and Kristjánsson, J. E.: Condensation and cloud parameterization studies with a mesoscale numerical weather prediction model, Mon. Weather Rev., 117, 1641–1657,1989.

Tanré, D., Kaufman, Y., Herman, M., and Mattoo, S.: Remote sensing of aerosol properties over oceans using the MODIS/EOS spectral radiances, J. Geophys. Res., 102, 16971–16988, doi:10.1029/96JD03437, 1997.

ACPD
14, 21975–22043, 2014

Taylor, K. E.: Summarizing multiple aspects of model performance in a single diagram, J. Geophys. Res., 106, 7183–7192, 2001.
Tompkins, A. M.: A prognostic parameterization for the subgrid scale variability of water vapor and clouds in large-scale models and its use to diagnose cloud cover, J. Atmos. Sci., 59, 1917–1942, 2002.
Tompkins, A. M.: The parametrization of cloud cover, ECMWF Moist Processes Lecture Note Series, available at: http://old.ecmwf.int/newsevents/training/lecture_notes/pdf_files/PARAM/Cloudcover.pdf (last access: 26 August 2014), 2005.
Tost, H., Jöckel, P., Kerkweg, A., Sander, R., and Lelieveld, J.: Technical note: A new comprehensive SCAVenging submodel for global atmospheric chemistry modelling, Atmos. Chem. Phys., 6, 565–574, doi:10.5194/acp-6-565-2006, 2006.
Tost, H., Jöckel, P., Kerkweg, A., Pozzer, A., Sander, R., and Lelieveld, J.: Global cloud and precipitation chemistry and wet deposition: tropospheric model simulations with ECHAM5/MESSy1, Atmos. Chem. Phys., 7, 2733–2757, doi:10.5194/acp-7-2733-2007, 2007a.
Tost, H., Jöckel, P., and Lelieveld, J.: Lightning and convection parameterisations – uncertainties in global modelling, Atmos. Chem. Phys., 7, 4553–4568, doi:10.5194/acp-7-4553-2007, 2007b.
Tost, H., Lawrence, M. G., Brühl, C., Jöckel, P.: The GABRIEL Team, and The SCOUT-O3-DARWIN/ACTIVE Team: Uncertainties in atmospheric chemistry modelling due to convection parameterisations and subsequent scavenging, Atmos. Chem. Phys., 10, 1931–1951, doi:10.5194/acp-10-1931-2010, 2010.
Twomey, S. A.: The influence of pollution on the shortwave albedo of clouds, J. Atmos. Sci., 34, 1149–1152, 1977.
Wang, J., Lee, Y.-N., Daum, P. H., Jayne, J., and Alexander, M. L.: Effects of aerosol organics on cloud condensation nucleus (CCN) concentration and first indirect aerosol effect, Atmos. Chem. Phys., 8, 6325–6339, doi:10.5194/acp-8-6325-2008, 2008.
Wang, M. and Penner, J. E.: Aerosol indirect forcing in a global model with particle nucleation, Atmos. Chem. Phys., 9, 239–260, doi:10.5194/acp-9-239-2009, 2009.
Weber, T., Quaas, J., and Räisänen, P.: Evaluation of the statistical cloud scheme in the ECHAM5 model using satellite data, Q. J. Roy. Meteor. Soc., 137, 2079–2091, 2011.
Wex, H., Petters, M. D., Carrico, C. M., Hallbauer, E., Massling, A., McMeeking, G. R., Poulain, L., Wu, Z., Kreidenweis, S. M., and Stratmann, F.: Towards closing the gap be-

ACPD
14, 21975–22043, 2014

tween hygroscopic growth and activation for secondary organic aerosol: Part 1–Evidence from measurements, Atmos. Chem. Phys., 9, 3987–3997, 2009, http://www.atmos-chem-phys.net/9/3987/2009/.

Wielicki, B. A., Barkstrom, B. R., Harrison, E. F., Lee III, R. B., Smith, G. L., and Cooper, J. E.: Clouds and the Earth's Radiant Energy System (CERES): an earth observing system experiment, B. Am. Meteorol. Soc., 77, 853–868, 1996.

Yoon, J., Burrows, J. P., Vountas, M., von Hoyningen-Huene, W., Chang, D. Y., Richter, A., and Hilboll, A.: Changes in atmospheric aerosol loading retrieved from space-based measurements during the past decade, Atmos. Chem. Phys., 14, 6881–6902, doi:10.5194/acp-14-6881-2014, 2014.

ACPD
14, 21975–22043, 2014

Table 1. Summary of the EMAC submodels used in this study.

Submodel name	Descriptions	Reference
AEROPT	Aerosol optical properties	Lauer et al. (2007)
CLOUD	Clouds and Precipitation	Jöckel et al. (2008)
CONVECT	Convection	Tost et al. (2010)
CVTRANS	Convective tracer transport	Tost et al. (2000b)
DRYDEP	Dry deposition of gases and aerosol	Kerkweg et al. (2006a)
GMXe	Aerosol dynamics and thermodynamics	Pringle et al. (2010)
HETCHEM	Heterogenous chemistry (reaction rates)	Jöckel et al. (2008)
JVAL	Rate of photolysis	Jöckel et al. (2006)
LNOX	Product of NO_x by lightning	Tost et al. (2007b)
MECCA1	Chemical atmospheric reactions	Sander et al. (2005)
OFFLEM	Offline emissions	Kerkweg et al. (2006b)
ONLEM	Online emissions	Kerkweg et al. (2006b)
RAD4ALL	Radiation for all wavelengths	Jöckel et al. (2006)
SATSIMS	Classification of cloud types by ISCCP simulator	Gerald et al. (2011)
SCAV	Wet deposition of gases and aerosols	Tost et al. (2006a, 2007a)
SEDI	Aerosol sedimentation	Kerkweg et al. (2006a)
TNUDGE	Tracer nudging	Kerkweg et al. (2006b)
TROPOP	Calculation of the tropopause and boundary layer	Jöckel et al. (2008)

ACPD
14, 21975–22043, 2014

Table 2. Description of aerosol size and number with seven aerosol modes and standard deviation (σ).

Aerosol Mode		Range of radius	sigma (σ)
Hydrophilic			
Nucleation	(NS)	$< 0.005\,\mu m$	1.59
Aitken	(KS)	$0.005\,\mu m < r < 0.06\,\mu m$	1.59
Accumulation	(AS)	$0.06\,\mu m < r < 0.5\,\mu m$	1.59
Coarse	(CS)	$> 0.5\,\mu m$	2.00
Hydrophobic			
Aitken	(KI)	$0.005\,\mu m < 0.06\,\mu m$	1.59
Accumulation	(AI)	$0.06\,\mu m < 0.5\,\mu m$	1.59
Coarse	(CI)	$> 0.5\,\mu m$	2.00

ACPD
14, 21975–22043, 2014

Table 3. Summary of main difference between the STN and HYB cloud microphysics (CDN) schemes.

Parameter	STAND (ARG)	HYBRID (ARG-κ)
Critical saturation	$s_{c,i} = 1 + S_{C,i}$	$s_{c_\kappa,i} = a_w \exp \frac{A}{D_i} = \exp\left(\sqrt{\frac{4A^3}{27\kappa_i D_i^3}}\right)$
Critical supersaturation	$S_{C,i} = \frac{2}{\sqrt{B_i}}\left(\frac{A}{3a_{c,i}}\right)^{\frac{3}{2}}$	$S_{C_\kappa,i} = s_{c_\kappa,i} - 1$
Kelvin effect	$A \equiv \frac{2\tau M_w}{\rho_w R T}$	$A \approx 0.66 \times 10^{-6} K\,m \times T^{-1}$
Solute effect	$\overline{B}_i \equiv \frac{M_w \sum_{j=1}^{J} r_{i,j}\mu_{i,j}\phi_{i,j}\epsilon_{i,j}/M_{a_{i,j}}}{\rho_w \sum_{i=1}^{J} r_{i,j}/\rho_{a_{i,j}}}$	$a_w = \frac{1}{1+\kappa_i\left(\frac{V_s}{V_w}\right)}$, $\kappa_i = \sum_{j=1}^{J} \hat{\epsilon}_{i,j}\kappa_j$

S_C is the critical saturation ($s_c \cong S_C + 1$) in STN and is comparable to S_{C_κ} ($= s_{c_\kappa} - 1$) in HYB.
a_c is the dry radius of the smallest activated aerosol and is used for estimating the fraction of aerosol activation.
M_w is the molecular weight of water vapor, ρ_w is the density of water; τ is the surface tension for water ($\tau = (76.10 - 0.155[T - T_{melt}])10^{-3}$) (Pruppacher and Klett, 1978), $R = 8.315\,J\,K^{-1}$ is the ideal gas constant, and T is temperature (K).
$r_{i,j}$ is the mass mixing ratio, $\mu_{i,j}$ is the number of ions after the salt dissociates into water, $\phi_{i,j}$ is the osmotic coefficient, $\epsilon_{i,j}$ is the mass fraction of soluble material, and $M_{a_{i,j}}$ is the molecular weight, $\rho_{a_{i,j}}$ is the density of the aerosol fraction of component j and mode i ($i = 1,7$).
a_w is the water activity, κ_i is the hygroscopicity of aerosol mode (i), the volume of the dry particle (V_s) and the volume of water (V_w).
$\hat{\epsilon}_{i,j}$ is the volume fraction of chemical component j in mode i, and κ_j is an independent hygroscopicity parameter of aerosol species (j).

ACPD
14, 21975–22043, 2014

Table 4. Summary of the sensitivity simulations.

Simulation	Cloud Droplet Nucleation parameterization	Cloud cover scheme
RH-REF	Fixed CCN concentration (REF)	Relative humidity cloud cover scheme (RH-CLC)
RH-STN	Standard CDN parameterization (STN)	RH-CLC
RH-HYB	Hybrid CDN parameterization (HYB)	RH-CLC
ST-REF	Fixed CCN concentration (REF)	Statistical cloud cover scheme (ST-CLC)
ST-STN	Standard CDN parameterization (STN)	ST-CLC
ST-HYB	Hybrid CDN parameterization (HYB)	ST-CLC

ACPD
14, 21975–22043, 2014

Table 5. Annual mean global mean cloud properties and TOA energy budget for 10 year simulations.

CDN scheme	No AIE inclusion		STAND (ARG)		HYBRID (ARG-κ)		Observed
Simulation	RH-REF	ST-REF	RH-STN	ST-STN	RH-HYB	ST-HYB	range
LWP ($g\,m^{-2}$)	44.3	24.9	93.2	75.4	61.2	38.1	37.8[a,1] 30–50[a,2]
IWP ($g\,m^{-2}$)	29.0	20.9	29.9	23.2	29.4	22.2	26.7[c,1],24–70[c,2]
N_d ($10^{10}\,m^{-2}$)	2.18	1.72	9.41	9.73	4.30	3.43	4[d]
N_i ($10^{10}\,m^{-2}$)	0.40	0.38	0.41	0.40	0.40	0.39	–
WVM ($kg\,m^{-2}$)	26.2	26.0	25.7	25.2	26.1	26.0	24.7 [b,1], 23[b,3]
TCC (%)	68.3	55.6	69.3	62.2	68.6	57.4	66.7[e,1], 65.4[e,2] %
P_{total} ($mm\,day^{-1}$)	3.01	2.97	2.96	2.95	3.00	2.97	2.68[f]
P_{start} ($mm\,day^{-1}$)	1.14	1.22	1.11	1.15	1.13	1.21	–
P_{conv} ($mm\,day^{-1}$)	1.87	1.75	1.86	1.80	1.87	1.76	–
SCRE ($W\,m^{-2}$)	−56.6	−33.6	−67.9	−52.1	−60.3	−38.9	−47.2[g] (−43.2 – −51.2)
LCRE ($W\,m^{-2}$)	28.5	24.3	28.7	25.5	28.6	24.7	26.3[g] (23.8–28.8)
AOD	0.20	0.19	0.23	0.22	0.21	0.19	0.16[h,1], 0.15–0.19[h,2]

[a] Liquid water path (LWP) and [b] water vapor mass (WVM) are from [1]CERES Terra SYN1 deg – lite Ed2.6 data for years 2001 to 2010 (Wielicki et al., 1996) and analysis of A-Train satellite observations [2] (from CloudSat (August 2006 to July 2010) and MODIS (October 2002 to September 2008)), [3] (AIRS (October 2002 to September 2010) + MLS (September 2004 to August 2011)) observation (Jiang et al., 2012).
[c] Ice water path (IWP) is from [1]ISCCP data (Storelvmo et al., 2008) and analysis of [2]CloudSat and MODIS observation (Jiang et al., 2012).
[d] Vertically integrated cloud droplet number (N_d) is drived by ISCCP (Han et al., 1994, 1998).
[e] Total cloud cover (TCC) is obtained [1]from Terra and Aqua MODIS data from the year 2000 to 2010 and [2]ISCCP data from 2001 to 2008.
[f] Total precipitation (P_{total}) is estimated by the Global Precipitation Climatology Project (GPCP) long term monthly mean for the years 1981 to 2010 (Adler et al., 2003).
[g] The shortwave, longwave and net cloud radiative effect (SCRE, LCRE and NCRE, respectively) at top of atmosphere (TOA) are estimated from the Clouds and the Earth's Radiant system experiments, Energy Balanced and Filled data (CERES EBAF) Ed2.6r for 2001 to 2010 (Loeb et al., 2009) (1° × 1° regional uncertainties, based on CERES EBAF Edition2.6r Data Quality Summary).
[h] Aerosol optical depth (AOD) is obtained from [1]CERES SYN1deg Month Terra Aqua MODIS Ed3A Subset from the year 2001 to 2010 and from [2]different observations (Kinne, 2006).

ACPD
14, 21975–22043, 2014

Table 6. Global means of activated aerosol fractions (AF_i) and CCN (CCN_i) in each mode, cloud droplet nucleation rate (R_{nuc}), and cloud droplet nucleation number (CDN) from the surface to upper troposphere (10 km) in large-scale clouds.

mode (i)	Aitken	Accumulation	Coarse	Total
Global	AF_{Atk}	AF_{Acc}	AF_{Cor}	R_{nuc}
RH-STN	20.1 %	59.9 %	61.7 %	$9.2 \times 10^{+3}$ m^{-3} s^{-1}
ST-STN	18.7 %	58.6 %	60.6 %	$8.4 \times 10^{+3}$ m^{-3} s^{-1}
RH-HYB	10.2 %	33.3 %	34.6 %	$4.3 \times 10^{+3}$ m^{-3} s^{-1}
ST-HYB	8.8 %	31.3 %	32.6 %	$3.7 \times 10^{+3}$ m^{-3} s^{-1}
Global	CCN_{Atk}	CCN_{Acc}	CCN_{Cor}	CCN_{total}
RH-STN	$8.3 \times 10^{+7}$	$3.5 \times 10^{+7}$	$0.5 \times 10^{+6}$	$1.3 \times 10^{+8}$ m^{-3}
ST-STN	$6.8 \times 10^{+7}$	$3.3 \times 10^{+7}$	$0.4 \times 10^{+6}$	$1.1 \times 10^{+8}$ m^{-3}
RH-HYB	$4.7 \times 10^{+7}$	$1.0 \times 10^{+7}$	$0.2 \times 10^{+6}$	$6.5 \times 10^{+7}$ m^{-3}
ST-HYB	$3.5 \times 10^{+7}$	$1.0 \times 10^{+7}$	$0.1 \times 10^{+6}$	$5.0 \times 10^{+7}$ m^{-3}

ACPD
14, 21975–22043, 2014

Table 7. Summary of locations and dominant aerosol types in the selected regions over the continents (CRs).

	Selected Continental Regions	Location	Dominant aerosol types
CR1	India and China	(80° E: 130° E, 10° N: 40° N)	SO_4 (DU, NO_3^-, NH_4^+, OC, BC)
CR2	Central Africa	(0: 40° E, 20° S: 15 ° N)	OC (BC, NO_3, NH_4^+)
CR3	Europe	(0: 80° E, 40° N: 60° N)	SO_4 (NH_4^+, BC)
CR4	North Africa and Arabian peninsula	(10° W: 60° E, 15° N: 40° N)	DU (SO_4, NH_4^+)
CR5	Brazil (Central South America)	(40° W: 80° W, 30° S: 10° N)	OC (BC, NO_3)
CR6	Sub Arctic and Siberia	(30° E: 120° E, 60° N: 75° N)	SO_4 (NH_4^+, BC)

ACPD
14, 21975–22043, 2014

Table 8. Estimated cloud radiative effects in the selected continental regions (CR) for SCRE, LCRE, and NCRE at TOA (corresponding to Fig. 9), and deviations and relative difference between the STN and HYB simulations [Rdiff = $\frac{\text{STN-HYB}}{\text{HYB}} \times 100(\%)$] and the sensitivity of the CLC scheme, defined as the ratio of relative differences [Sensitivity = $\text{Rdiff}_{ST}/\text{Rdiff}_{RH}$].

	SCRE ($W\,m^{-2}$)				Deviation Δ (STN-HYB)		Relative difference (%)	
	RH-STN	ST-STN	RH-HYB	ST-HYB	ΔRH (STN-HYB)	ΔST (STN-HYB)	Rdiff_{RH}	Rdiff_{ST}
CR1	−75.8	−73.7	−62.4	−47.1	−13.5	−26.6	21.6	56.5
CR2	−59.5	−57.7	−55.7	−37.5	−3.8	−20.2	6.8	53.8
CR3	−45.3	−49.7	−35.1	−29.2	−10.3	−20.4	29.3	69.9
CR4	−12.3	−11.1	−11.1	−9.8	−1.2	−1.3	10.5	13.1
CR5	−81.5	−76.0	−69.7	−42.0	−11.9	−34.1	17.1	81.2
CR6	−57.3	−59.6	−41.6	−31.3	−15.7	−28.4	37.6	90.8
	LCRE (W/m^2)				Deviation Δ (STN-HYB)		Relative difference (%)	
	RH-STN	ST-STN	RH-HYB	ST-HYB	ΔRH (STN-HYB)	ΔST (STN-HYB)	Rdiff_{RH}	Rdiff_{ST}
CR1	33.4	29.9	36.7	35.4	−3.3	−5.5	−8.9	−15.5
CR2	29.7	27.6	35.6	40.7	−6.0	−13.1	−16.7	−32.2
CR3	26.6	25.3	27.6	24.7	−1.0	0.6	−3.8	2.5
CR4	17.1	13.5	16.1	14.1	1.0	−0.6	6.1	−4.1
CR5	32.9	30.7	36.5	38.9	−3.6	−8.2	−9.8	−21.0
CR6	21.9	21.5	23.4	22.0	−1.5	−0.5	−6.2	−2.1
	NCRE ($W\,m^{-2}$)				Deviation Δ (STN-HYB)		Sensitivity	
	RH-STN	ST-STN	RH-HYB	ST-HYB	ΔRH (STN-HYB)	ΔST (STN-HYB)	SCRE	LCRE
CR1	−42.4	−43.7	−25.7	−11.6	−16.7	−32.1	2.6	1.7
CR2	−29.8	−30.1	−20.1	3.2	−9.8	−33.3	7.9	1.9
CR3	−18.8	−24.4	−7.5	−4.6	−11.3	−19.8	2.4	−0.7
CR4	4.9	2.3	5.0	4.2	−0.2	−1.9	1.2	−0.7
CR5	−48.6	−45.3	−33.2	−3.1	−15.4	−42.3	4.8	2.2
CR6	−35.3	−38.1	−18.2	−9.3	−17.1	−28.9	2.4	0.3

ACPD
14, 21975–22043, 2014

Table 9. Evaluation of the performances of the CDN and CLC schemes in the EMAC model based on the statistical analysis (i.e., standard deviation and correlation coefficient).

	Continental						Marine					
RH-CLC	TCC	SCRE	LCRE	Ptot	AOD	Sum (Ave.)	TCC	SCRE	LCRE	Ptot	AOD	Sum (Ave.)
RH-REF	5	4	4	4	3	20 (4.0)	4	3	4	2	2	15 (3.0)
RH-STN	4	2	3	2	3	14 (2.8)	4	2	3	2	1	12 (2.4)
RH-HYB	5	3	4	4	3	19 (3.8)	4	2	4	2	2	14 (2.8)
ST-CLC	TCC	SCRE	LCRE	Ptot	AOD	Sum (Ave.)	TCC	SCRE	LCRE	Ptot	AOD	Sum (Ave.)
ST-REF	4	3	4	1	4	16 (3.2)	2	3	4	2	2	13 (2.6)
ST-STN	4	2	3	4	3	16 (3.2)	3	2	4	2	2	13 (2.6)
ST-HYB	4	4	4	2	3	17 (3.4)	2	2	4	3	2	13 (2.6)

Rating is based on the calculated skill score (S), see Table S2.

ACPD
14, 21975–22043, 2014

Table 10. Global means of convective cloud top height (CTH) (unit: m) and convective available potential energy (CAPE) (unit: J kg^{-1}) over land and ocean, based on daily (24 h) means.

Continental						
LAND	RH-REF	RH-STN	RH-HYB	ST-REF	ST-STN	ST-HYB
CTH (m)	1346	1229	1323	1395	1179	1381
CAPE (J kg^{-1})	24.41	18.70	23.26	32.59	20.91	31.19
		RH (STN-REF)	RH (HYB-REF)		ST (STN-REF)	ST (HYB-REF)
Relative difference	CTH	−8.69 %	−1.71 %	CTH	−15.48 %	−1.00 %
	CAPE	−23.39 %	−4.71 %	CAPE	−35.84 %	−4.30 %
Marine						
OCEAN	RH-REF	RH-STN	RH-HYB	ST-REF	ST-STN	ST-HYB
CTH (m)	1234	1271	1249	1084	1165	1097
CAPE (J kg^{-1})	32.41	34.35	32.93	27.61	32.22	28.04
		RH (STN-REF)	RH (HYB-REF)		ST (STN-REF)	ST (HYB-REF)
Relative difference	CTH	3.00 %	1.22 %	CTH	7.47 %	1.20 %
	CAPE	5.99 %	1.60 %	CAPE	16.70 %	1.56 %

ACPD
14, 21975–22043, 2014

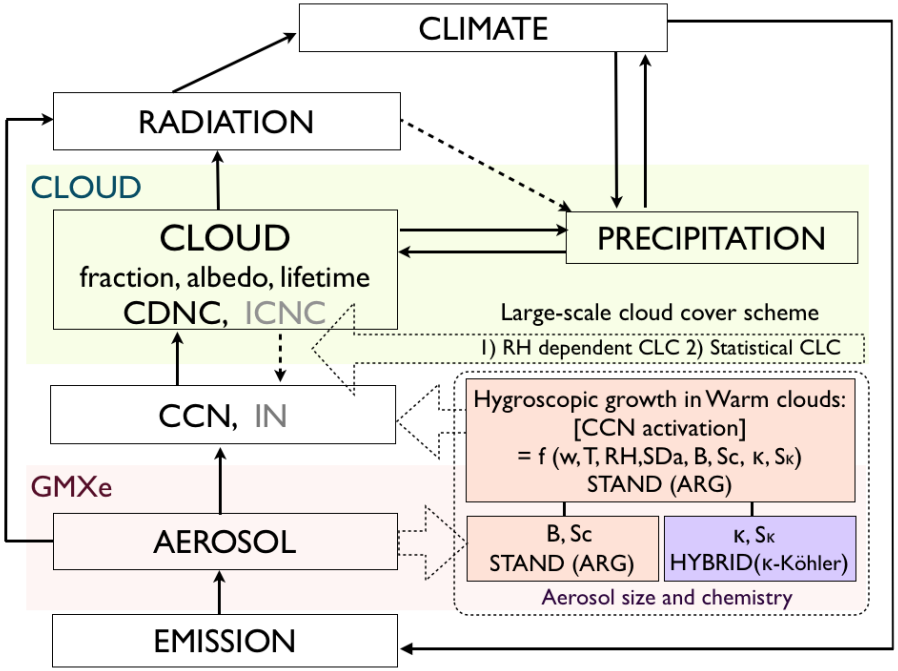

Figure 1. Overview of the EMAC model structure used in the present study: ω (vertical motion), T (temperature), RH (relative humidity), SD_a (size distribution of ambient aerosol), B (hygroscopicity), S_c and S_κ (critical supersaturation), κ (effective hygroscopicity parameter).

ACPD
14, 21975–22043, 2014

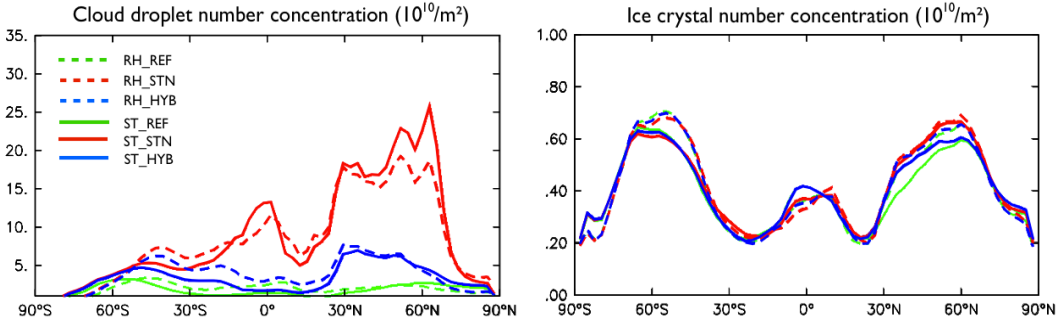

Figure 2. Annual, zonal means of vertically integrated cloud droplet number concentration (N_c) and ice crystal number concentration (N_i) in the REF (green), in the STN (red) and HYB (blue) simulations described in Table 4. Dashed lines refer to the RH cloud cover scheme (RH-CLC) and solid lines to the statistical cloud cover scheme (ST-CLC).

ACPD
14, 21975–22043, 2014

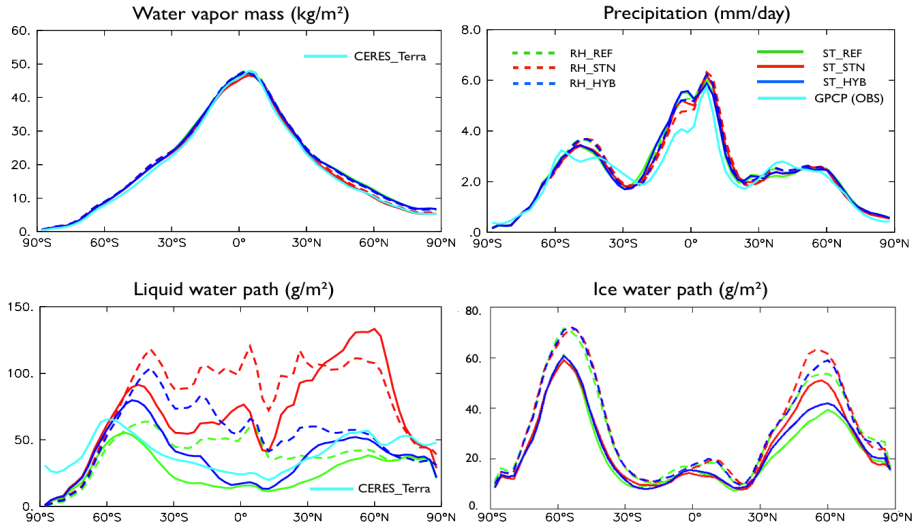

Figure 3. Annual, zonal mean water vapor mass (WVM), total precipitation (P_{tot}), liquid water path (LWP), and ice water path (IWP). The dashed and solid lines refer to RH-CLC and ST-CLC, respectively; and the green, red and blue colors represent REF, STN and HYB, respectively. The light blue lines show observations.

ACPD
14, 21975–22043, 2014

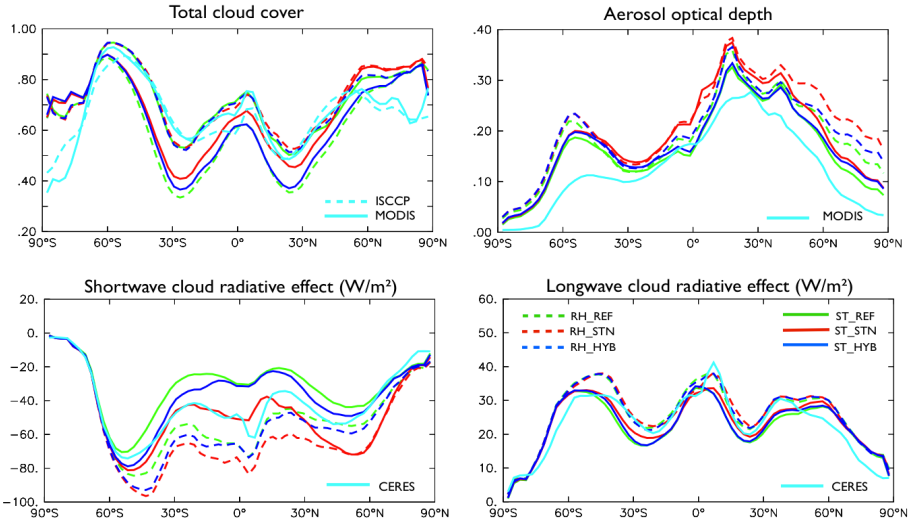

Figure 4. Annual, zonal means of the total cloud cover (TCC), aerosol optical depth (AOD), short wave cloud radiative effect (SCRE) and longwave radiative effect (LCRE) at the top of the atmosphere (TOA) shown with the same colors and line symbols as Fig. 3.

ACPD
14, 21975–22043, 2014

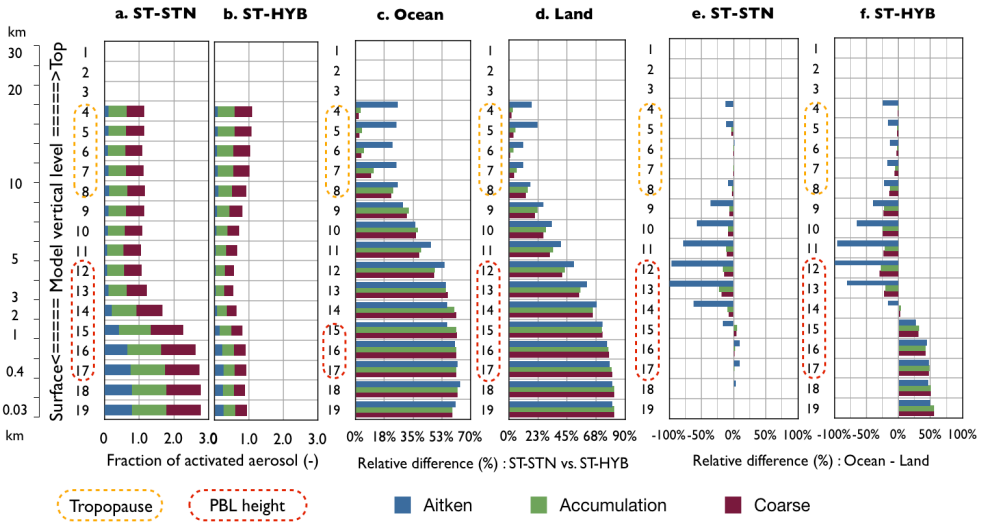

Figure 5. Vertical distributions of global means of the activated aerosol fraction for **(a)** ST-STN and **(b)** ST-HYB, the relative difference between the ST-STN and ST-HYB over the ocean **(c)** and the continent **(d)**. The relative differences between the oceans and the continents in ST-STN **(e)** and ST-HYB **(f)** are shown for the Aitken, accumulation and coarse modes denoted by the blue, green and red colors, respectively. The dashed yellow and red lines (left) are latitudinally varying ranges of the tropopause and the planetary boundary height, respectively.

ACPD
14, 21975–22043, 2014

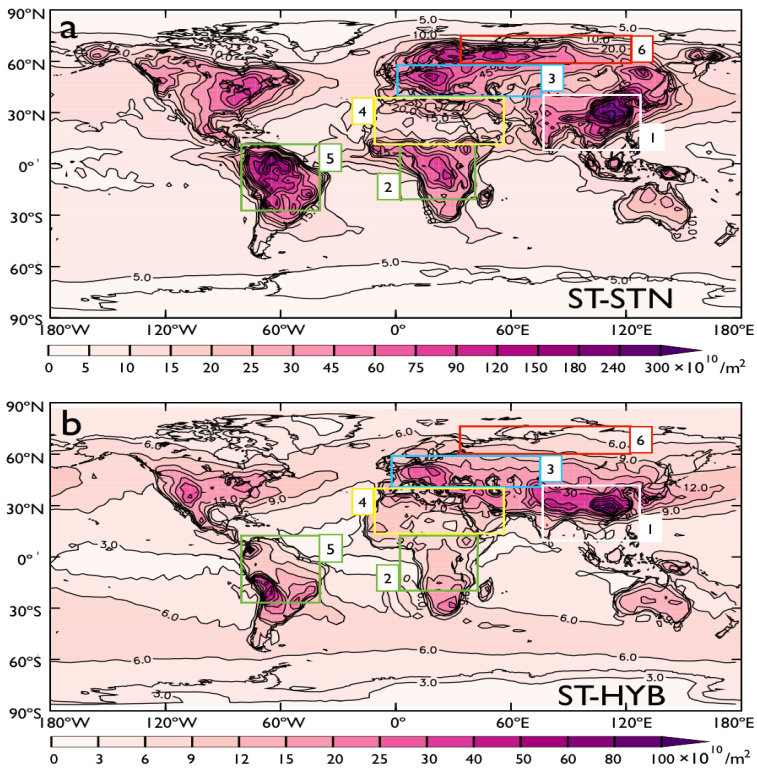

Figure 6. Global distributions of cloud droplet number concentration (CDNC) in **(a)** ST-STN and **(b)** ST-HYB.

ACPD
14, 21975–22043, 2014

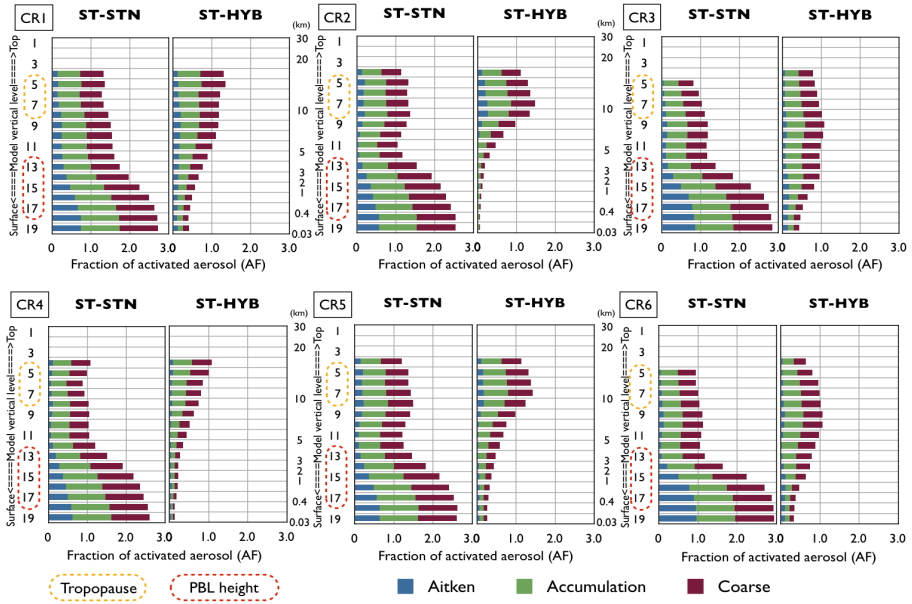

Figure 7. Vertical distributions of the CCN activation fractions in the selected continental regions (from CR1 to CR6) for ST-STN and ST-HYB.

ACPD
14, 21975–22043, 2014

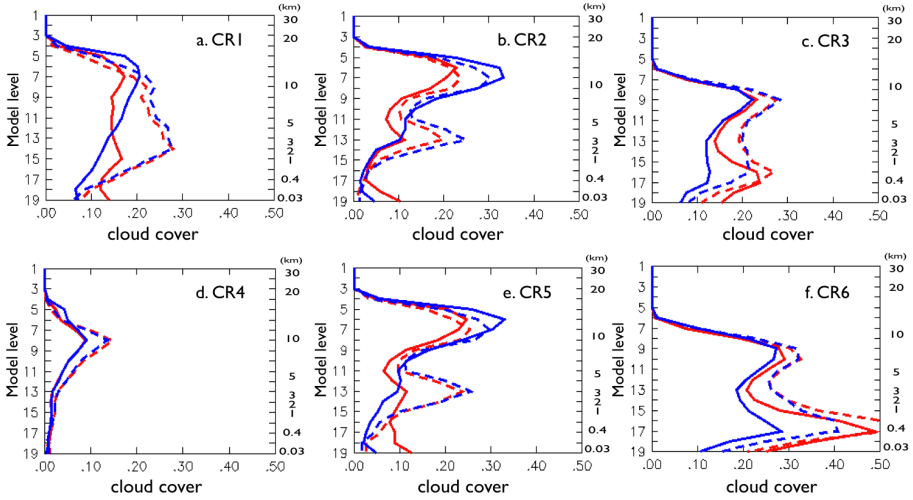

Figure 8. Vertical distributions of cloud cover in the selected continental regions (CR) for RH-STN, ST-STN, RH-HYB, and ST-HYB, presented with the same colors and lines as in Fig. 5.

ACPD
14, 21975–22043, 2014

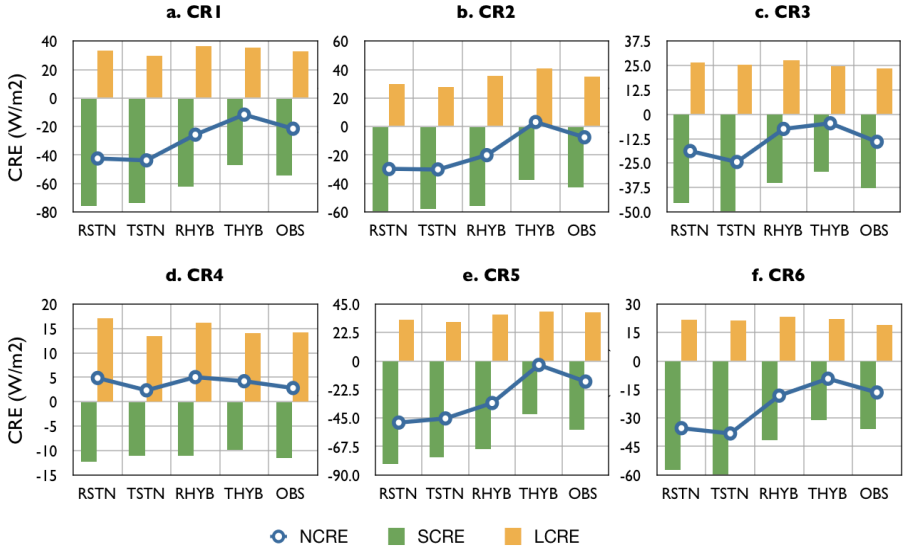

Figure 9. Cloud radiative effects in the selected continental regions (CR) for RH-STN (RSTN), ST-STN (TSTN), RH-HYB (RHYB), and ST-HYB (THYB), presented with a green, yellow bar and blue line representing the SCRE, LCRE and NCRE at TOA, respectively.

ACPD
14, 21975–22043, 2014

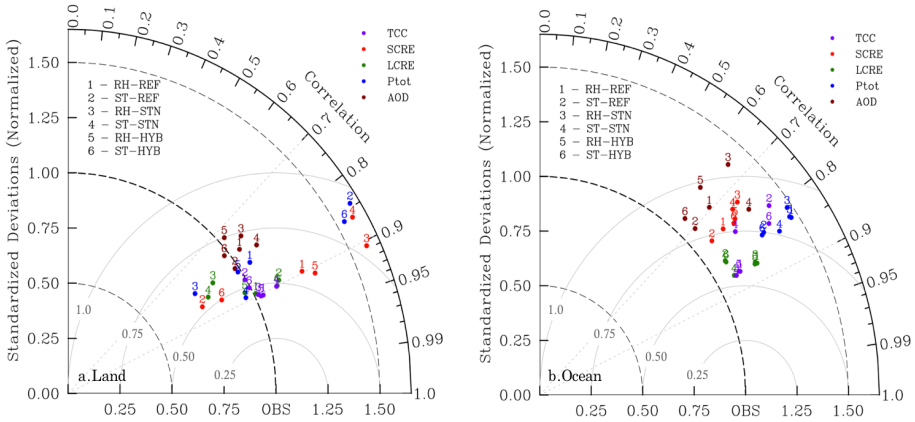

Figure 10. Taylor diagrams with a statistical comparison between model results and observations as described in Table 5; over land **(a)** and over ocean **(b)**; the SCRE and LCRE at TOA in CERES EBAF, the total precipitation (P_{tot}) in GPCP, the total cloud cover between 60° S and 60° N (TCC) and the aerosol optical depth (AOD) both from MODIS.

ACPD
14, 21975–22043, 2014